Battery Energy Storage Systems

- Power Electronic Solutions and Control -

Project Report

IEL5-E23

Aalborg University
AAU Energy

LaTeX used for formatting.

Energy Department
Aalborg University
http://www.aau.dk

AALBORG UNIVERSITY
STUDENT REPORT

Title:
Battery Energy Storage Systems:
Power Electronic Solutions and Control

Theme:
Automation including Power Electronics

Project Period:
Autumn Semester 2023

Project Group:
IEL5-E23

Participant(s):
Boris Fabula
Nils Albin Emil Nolemo
Miguel Ángel García Otalora

Supervisor(s):
Amin Hajizadeh

Copies: 1

Page Numbers: 53

Date of Completion:
February 7, 2024

Abstract:

The accelerating electrification in society has lead to a large increase in battery usage in a variety of sectors including transportation, energy and heavy industry. The possibility of re-purposing and re-using decommissioned batteries in Battery Energy Storage Systems could greatly reduce the environmental impacts of battery production by extending their lifespans.
One way to use them is as peak shaving storage, whereby batteries could be charged during overproduction when electricity prices drop and act as a supply when prices peak. This could both be an economically beneficial venture as well as assist with the challenges of grid instability from renewable energy sources. With this purpose in mind, the project aims to investigate the following areas:

- Analysing the economic feasibility of using second-life batteries for peak shaving purposes.
- Modelling and control of power electronic circuits for converting AC into a controllable DC output.

Contents

Preface

This report was done by a fifth semester group of the Applied Industrial Electronics program at Aalborg University in Esbjerg. The project was completed as part of fulfilling the curriculum for the project course **Automation including Power Electronics**.

Aalborg University, February 7, 2024

Boris Fabula
<bfabul21@student.aau.dk>

Nils Albin Emil Nolemo
<nnolem21@student.aau.dk>

Miguel Angel Garcia Otalora
<maga21@student.aau.dk>

Chapter 1

Introduction

Energy storage is set to become an increasingly important tool to secure energy access and stability in the grid. The increasing electrification of society and the growth of variable power sources necessitate new ways of handling the greater demand and greater instability of the electricity supply. One of the ways in which this storage capacity may be expanded is to implement second-life batteries (SLB) as energy storage. According to the Mckinsey Center for Future Mobility, energy storage using electric vehicle SLBs could by 2030 have a capacity of over 200GWh[1].

The future of energy storage is being developed both on the legislative front and the technical front. The European Commission in a recommendation issued in 2023 highlighted that storage of energy could be a part of the solution to the technical challenges of increasing renewables in the energy mix. Additionally, the report points out that storage could be used to reduce costs for consumers, and lower dependence on fossil fuel imports to remote regions[2]. An example of an already implemented technical solution in this area is in Almería, Spain, where SLBs have been installed as a storage unit alongside the local thermal power plant to improve the energy supply in the city[3].

Given the outlook and growth in this area, the initiating problem for this project to guide further research into the area was defined as:

> How can SLB be implemented in a business scenario as a solution to reduce energy costs?

Chapter 2

Problem Analysis

2.1 Introducing Battery Energy Storage Systems (BESS)

BESS are stations that contain an array of rechargeable batteries, as well as the necessary components like power converters, filters and control systems to connect the battery array to different energy sources and loads[4]. The purpose is to store and discharge energy strategically. The system can be off-grid (typically connected to solar or wind sources), grid tied, or interact with both renewables and the grid. Installing a BESS can be beneficial across multiple areas of industry and business for reasons such as:

- Grid resilience - ability to recover from unexpected issues[5]
- Optimisation of renewable energy plants as an example of grid balancing - accumulating overproduction from wind and solar plants to deliver it when the weather is sub-optimal[6]
- Peak shaving - Rapid expansion of EV charging stations could increase the load beyond what the grid was initially designed for. BESS can spread the peak load over a longer period that stays within limitations of the grid[7]
- Energy arbitrage - buying electricity during cheaper periods to charge a BESS and sell it back to the grid when prices peak[8]

Because of these points, BESS can be of interest for electricity distribution companies to improve the grid stability by decentralisation of energy sources, and to increase the capacity of the grid to accommodate for peak demands that can result from e.g. installing EV charge stations at places like shopping malls[7]. Furthermore, BESS can be implemented

in renewable energy plants to stabilise the fluctuations of energy output caused by e.g. cloud cover. Similarly, batteries can be used instead of auxiliary peaking power plants that usually run on fossil fuel to stabilise the grid during peak demand[9]. This could assist in achieving international goals of lowering emissions[10]. From an economical perspective, BESS can be used for energy arbitrage, meaning the energy can be stored at a lower price per kWh and later delivered during periods of increased rate. Such usage could be interesting for industry, factories, or office buildings, shopping malls and also supermarkets, which will be further analysed in this report.

2.1.1 Key components of BESS

A typical configuration of a grid-tied BESS can be described as in Figure 2.1.

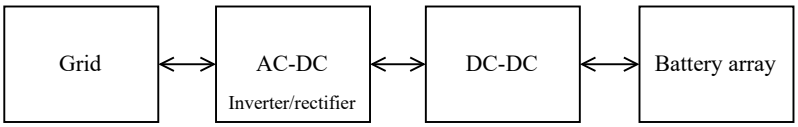

Figure 2.1: Block diagram showing key components of a BESS[11]

- **The grid** The system is connected either to a three-phase grid or works on a single phase.
- **Inverter/Rectifier** Converts voltages from DC to AC, when providing electricity to the grid is required and from AC to DC to charge the batteries.
- **DC-DC converter** Brings the signal from the rectified DC level to the input required at any given moment during the charging cycle of the battery array as well as the voltage delivered by the batteries to a suitable level for the inverter.
- **Battery array** Central piece of the station, all the other components must work to ensure, an adequate performance with a long life. Given that battery packs typically come as a combination of series and parallel cell groups, a battery management system (BMS) is needed for balance charging and monitoring the health of the batteries to detect possible issues.

It is worth noting that there exist multiple BESS configurations and not all of them include a DC-DC converter stage [12]. Another important requirement a BESS must fulfil is providing galvanic isolation to protect personnel, equipment, and to adhere to regulations and standards [13]. Isolation could be implemented either prior to the AC-DC conversion, at the inverting/rectifying stage or at the DC-DC converter stage.

2.1.2 Use of BESS in supermarkets

A short list of possible benefits of using a BESS was introduced in Section 2.1. Various industries and areas of business could profit from these, but this report investigates the economic advantage of using a BESS in supermarkets.

There exist some BESS with SLB implementations in the retail industry. The Czech automobile manufacturer Škoda is installing power hubs at their retailers, which uses end-of-life lithium-ion batteries as storage. These batteries are taken from the brand's vehicles, and according to Škoda this could extend the useful life of the batteries by up to 15 years. The system has a total capacity of 328 kWh[14].

In the United States there are several startups which in recent years are repurposing used batteries from Nissan vehicles[15]. One of them received public funding to install solar photovoltaic and energy storage microgrid systems at co-op grocery stores[16].

From an economical point of view, sizing energy expenses is a key factor for retailers to keep points of sale operating or closing them. Denmark presents a very competitive market where margins fall usually under 5%[17], which has led some national retailers to close and transnational ones to exit the country, like Irma in 2023[18] and Aldi in 2022[19]. Despite historically not being one of the main cost drivers for grocers, the growing tension of energy prices in Europe is also affecting them, and led some retailers into protesting by switching off illumination and coolers[20].

A distinctive factor in the Danish sector that contributes to energy consumption is the legal limitation on the plant size to 5000 m^2[21] which contributes to smaller, more evenly distributed stores rather than big hypermarkets. Smaller supermarkets tend to have greater energy consumption[22].

The average energy use intensity for supermarkets in Denmark, Sweden, and The Netherlands is 400 kWh/m^2/year[22] while in the United Kingdom it is 450 kWh/m^2/year[23]. For similar environmental conditions, the energy consumption of the supermarket will vary depending on the ratio of frozen to chilled products and on the refrigeration system. Plug-in cabinets and R134a centralised systems are widely used, while in recent years there is a growing use of trans-critical CO2 booster system, which could lead into energy savings. In all cases refrigeration takes the biggest share on the bill, then HVAC, heating, and cooling[24]. Besides geographical location, sales area, refrigeration system topology, and installed capacity, opening hours have also and major impact on the performance. Other minor indicators are sales volume, year of construction or refurbishment, management, and system control[25].

2.2 Problem definition

A BESS is a variable system that can be used for different purposes, as described in Section 2.1. This project focuses on electricity arbitrage by supermarkets with the aim of lowering electricity costs. A BESS is proposed to charge while the price of electricity is the lowest and deliver the energy during the period when the rate peaks. To assess the viability of this solution, an economical analysis of a system based on second-life batteries is performed on a model of an average supermarket. Moreover, the developed model is simulated in Simulink and a prototype is built to practically test a power electronic circuit.

2.3 Problem delimitation

In the context of a semester project centered around automation and power electronics, multiple parts of a BESS can be researched for the group to gain the expected knowledge, skills and competences. Considering that state-space modelling, digital control and prototype development should be achieved, a section of a complete BESS set-up is selected. The technical focus in this report is the power electronic circuits necessary to take a single-phase AC input and convert it to a desired DC output value using a controller. Hence the model is designed to deliver power one way from grid to battery.

As with all electrical systems, efficiency is of great importance in a BESS. The efficiency of the system will impact the economic viability and outcome of such a setup. Any loss of energy in conversion and storage processes has a negative impact on the main goal of lowering the final price of consumed electricity and payback period. However, the proposed prototype focuses on learning objectives, simplicity of implementation and should rather be considered a proof of concept than a solution showing high efficiency. Nevertheless, efficiency of the prototype is considered for exercising economic analysis.

Chapter 3

Economic Analysis

3.1 Supermarket model

To define the BESS specifications it is necessary to retrieve the energy requirements of the building. This can widely vary depending on factors such as location, target population size, season of the year, or efficiency of the equipment. To find a simple to implement yet representative requirements, an ideal, average Danish supermarket is defined. The definition comes from the average surface of a supermarket in Denmark, 611m^2 multiplied by the average energy intensity of 400 kWh/m^2/year discussed in section 2.1.2 [26]. The ideal supermarket model will consume 244,4 MWh/year or 669,14 kWh/day. At 230V AC input to the store, this means an average current of around 122A.

3.2 Storage capacity

Defining the capacity of the BESS is done by inspecting electricity cost data available from the Danish Energinet data service[27], where energy prices were found per hour from 1/10/2022 to 1/10/2023 and the average hourly price was taken, giving the data in figure 3.1.

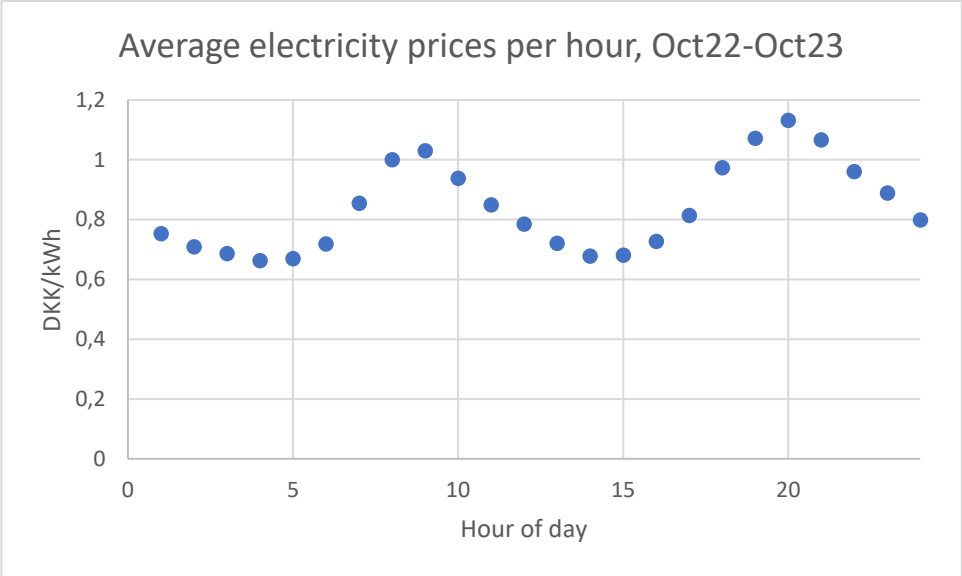

Figure 3.1: Plot showing the average electricity price per hour in Denmark of the days over the period between 1/10/2022 to 1/10/2023.

Due to the fact that tax-registered companies in Denmark can claim energy fees back, taxes are not taken into consideration[28]. A visible trend can be seen with a morning spike and evening spike, particularly in the evening hours of 19-21 where the prices are significantly higher. Given this spike, it was decided to design the capacity of the batteries to accommodate five hours of run time of the store in order to be able to cover the peaks. At a consumption of 669,14 kWh/day, this means a minimum capacity of 140 kWh.

3.3 Sourcing of second-life batteries

The sourcing of SLBs will become a critical issue if they are to become widely adopted in different industries. By sector, industrial batteries and automotive batteries account for an estimated total of around 70% of the world market share of the battery sector[29]. In the industrial sector, a mix of lead based and lithium based batteries are expected to be present in the future, while in the automotive sector lithium based is expected to be the most widely used[30]. It is however anticipated, that the main focus within the future SLB industry will be used electric vehicle batteries due to the global increase in sales of electric vehicles[31].

Despite the likely future availability of SLBs there are some anticipated problems with utilising these. One of the issues is lack of standardisation. Batteries are made in many different configurations and chemistries, meaning that all SLBs cannot be treated and used

equally[1]. There are however organisations working on forming standards for the battery industry to ease issues like this in the future[32]. Another potential issue in the sourcing of SLBs is the competition with newly produced cells. Battery prices have been falling rapidly in the last decade, with lithium-ion battery costs in 2010 over 1100 USD/kWh, to prices of around 137 USD/kWh in 2020[33]. This falling price poses the risk of causing SLBs to become economically non-viable, as they can have cost factors associated with them such as performance screening, disassembly, reassembly and so forth[34]. National Renewable Energy Laboratory estimated in 2015 that the cost of refurbished second-life batteries could vary widely between around 44 USD/kWh to 180 USD/kWh, of which the repurposing and processing costs were then estimated between 25 USD/kWh and 49 USD/kWh[35]. This means that the refurbishing is a significant part of the cost for SLBs. With the price of new lithium batteries at around 137 USD/kWh, the price of used cells would have to be significantly lower than this to make purchasing them instead of new batteries an economically viable decision. Technological advancements can also accelerate the imbalance in value between used and new batteries. This could be corrected by implementation of regulation and tax rebates for systems using refurbished batteries[34].

3.4 Preliminary economic analysis

In order for the system to be of use in a business scenario, it needs to be economically viable. Unless the savings in energy costs can pay off the initial equipment costs over some defined time period, it is not a worthwhile investment. To do a preliminary analysis of this, some parameters must be assumed and set. It is necessary to make assumptions about the upfront cost of the equipment, what time frame is acceptable for paying off the upfront cost, and the longevity of the equipment and batteries.

As described in Section 3.2, the minimum required storage capacity necessary for the considered average supermarket is 140kWh. Additionally, the average degradation of EV batteries stands at around 2,3% per year[36]. If the minimum capacity of 140kWh is to be maintained for at least 10 years, a capacity of $140/(1-0,023)^{10} = 177$ kWh is required to compensate for the degradation. Moreover, the end-of-life State-Of-Health (SOH) for EV batteries is around 80%[1]. Assuming that SLBs will be sold with around 80% capacity, EV batteries with an original capacity of at least 177 kWh/0,8 = 222 kWh are needed. To cover the current requirement of 122 A for a period of 5 hours and capacity requirement of 222 kWh when new, the battery model can be based on a common battery present in the market such as the Tesla Model 3 long range model, which has a battery pack with a capacity of 230 Ah or 80,5 kWh[37]. Three of these packs in parallel connection would cover the requirement for the supermarket BESS, giving an overall capacity of 690 Ah or 241,5 kWh at 100% SOH. At refurbishing prices between 44 and 180 USD/kWh as described in Section 2.2, the price for the required SLB could be between 10867 and 43470

USD at current estimates.

Besides batteries, equipment such as power converters, rectifiers/inverters and transformers are necessary to be able to charge and discharge the batteries. Finding pricing information on these is difficult due to the fact that pricing from manufacturers of these components is usually done on a case by case basis. Acquiring an accurate figure for the price of this equipment would necessitate fully designing the system and engaging in talks with vendors to obtain the prices. This is outside of the time scope of this project, and thus the equipment price will be assumed to equal that of the battery price, giving a range of 10626 to 43470 USD, or 73957 to 303303 DKK as per 09/11/2023 exchange rates[38].

Using the electricity pricing in Section 3.2, the total average cost per month is calculated by multiplying each price per hour by 30 days $\cdot$ 1/24 hours $\cdot$ 670 kWh/day and summing all 24 values, giving a total electricity cost of 16895 DKK/month. To estimate the amount that could be saved by load shifting for a total of 5 hours per day, the calculation is redone, but exchanging the 5 highest cost hours for the 5 lowest. Redoing the same calculation yields a monthly cost of 15286 DKK. This is a saving of 1609 DKK/month, or 10,1% of the original cost.

Using the gathered information of battery price, equipment price and potential savings, a range of possible payback time is calculated and shown in table 3.1.

Table 3.1: Potential costs and payback time for the BESS in an average danish supermarket.

		Low case	High case
Battery cost	(DKK)	73957	303303
Total cost	(DKK)	147914	606606
Payback time	(years)	7,66	31,4

It is important to emphasise that the figures used contain assumptions regarding pricing. The battery prices are an estimate of what the price may be in the future, and the equipment pricing is an assumption made due to lack of information. Assuming these to be close to reality, the feasibility of this system would be up to the individual supermarket chains on what range of time they expect return on investment. The lower end of 7,66 years does not seem an unreasonable one if factored in that reuse of batteries would not only be an economic benefit, but also an environmental one. Additionally, there are ways that these types of use cases could be incentivised through tax credits similar to that which has been done with electric vehicles and charging installations in Sweden[39]. Another potentially beneficial incentive is that of smart grid applications whereby energy can be bought and sold to energy distributors during high demand times to help balance the grid[40].

Chapter 4

Problem Solution

In this chapter, possible converter topologies as well as voltage busses are discussed, necessary mathematical models derived, a controller developed, and a Simulink model is proposed for controller tuning and analysis.

A conventional on-grid charging solution consists of two stages: an AC-DC rectifier followed by a DC-DC converter. For each stage, different conversion topologies exist.

The first stage is converting AC from the grid to DC for which several options are available. There are two main categorisations of single-phase rectifiers: uncontrolled and controlled[41].

- Uncontrolled rectifiers
  In this topology there is no control over output voltage. These can be half-wave, where only half of the AC sine wave is converted to DC, or full-wave were the whole period of the sine wave is converted into DC. Their advantage is their simplicity of implementation, while their main drawback, despite the lack of control, is their low efficiency.
- Controlled rectifiers
  In this topology a switch (MOSFET, IGBT, or SCR) is used in conjunction with a switching signal for every pair of transistors, typically PWM signals are used for this purpose.

The chosen topology is a controlled rectifier, because of its higher efficiency. The next design choice regarding the AC-DC conversion is the type of DC-Bus[13].

- Variable DC-Bus
  As battery voltage varies with its state of charge, a variable output voltage is required

when charging. With a variable DC-bus the battery is connected directly to the DC-bus that follows the battery voltage. This saves the need for a DC-DC stage, lowering the cost of the system. The downside is that scalability is lower than with a constant DC-Bus, since a different type of battery can not be connected to the same bus directly. To expand the system, isolated DC-DC converters are required. As the bus is varying, the converters need a wide input voltage which can affect their efficiency.

- Constant DC-Bus
  With a constant bus, the battery in the system requires a DC-DC converter, which can be non-isolated if isolation is provided in a previous stage. Using isolated DC-DC converters allows for higher scalability.

A constant DC-Bus is chosen for its simplicity, which requires the use of a versatile DC-DC converter which can supply the batteries with varying voltages throughout their charging cycles. The main topologies for DC-DC converters [42][43] are:

- Buck Converter
  Step-down converter where the voltage output is lower than the input.
- Boost Converter
  Step-up converter where voltage output is higher than the input.
- Buck-Boost Converter
  Can step up (boost) or step down (buck) the input voltage. Produces an inverted output.
- Cùk Converter
  Similar to the buck-boost converter, includes an additional capacitor for reduced ripple. Produces an inverted output.
- Flyback Converter
  With a similar design to the buck-boost, the flyback converter uses a transformer, instead of an inductor to store energy for the conversion.
- Full-Bridge Converter
  Utilises a bridge circuit with active switches (MOSFET, IGBT, or SCR) for bidirectional power flow.
- SEPIC Converter
  The single-ended primary-inductor converter (SEPIC) consists of a series connection of a boost converter and an inverted buck-boost converter. It behaves like a buck-boost with the advantage of producing a non-inverted output.

Since the use of a constant DC-Bus on the rectifier requires a DC-DC converter that can both buck and boost. Satisfying this criterion, the buck-boost is chosen for having fewer components which facilitated both the modelling and physical implementation. Negative voltage output is the main drawback of this topology and is discussed further in the report.

The decisions made in this section are summarised in the block diagram in Figure 4.1.

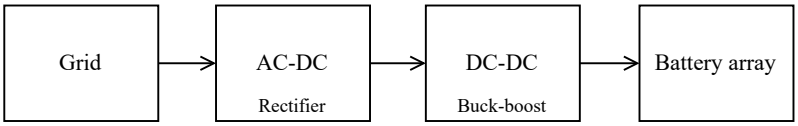

Figure 4.1: Block diagram showing the focus of the report.

4.1 Modelling

As the chosen rectifier is of constant DC-bus, where the firing angle does not vary, there is no control involved. Therefore, there is no need for developing a model for it, whereas the controlling importance lies on the buck-boost converter. It has to be able to react to different reference voltages and stabilise them. To develop a proper controller, a mathematical model is required.

4.1.1 Buck-boost converter

In order to develop a control loop and control the output of the buck-boost converter, a model based on a duty-cycle to output voltage transfer function is required. The buck-boost converter model is derived using state space averaging method and small signal analysis[44].

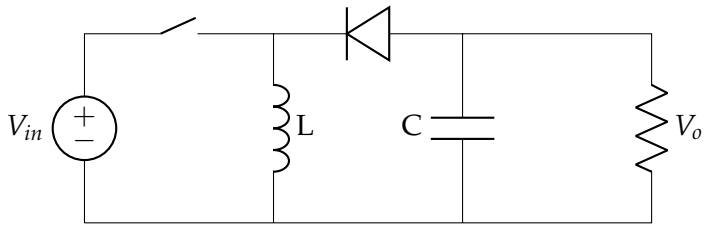

(a)

Figure 4.2: Buck-boost converter

The buck-boost converter circuit in Figure 4.2 can be split up in two different scenarios

depending on the switch being open or closed as shown in Figure 4.3

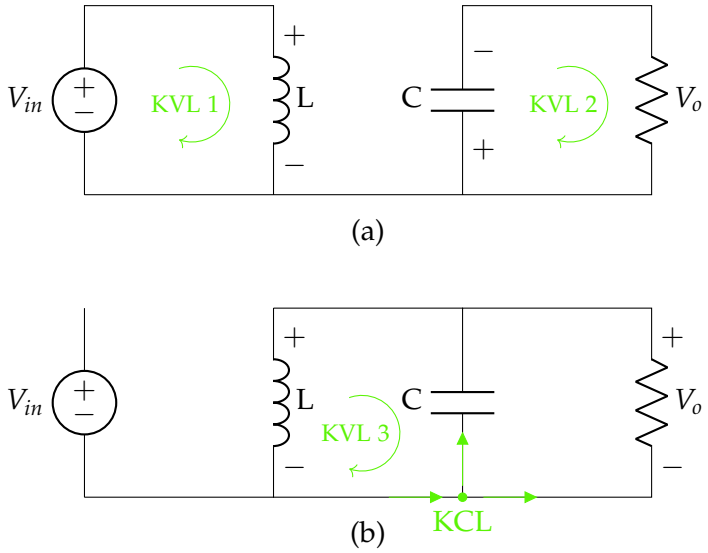

Figure 4.3: Circuit modes for the buck-boost converter: (a) On mode (b) Off mode

Depending on the switch being open or closed, two separate state space models can be derived. For both states, Kirchhoff's voltage and current law (KVL and KCL) are used to derive equations describing them, where inductor current and capacitor voltage are taken as the states and output voltage as the output. For the on scenario, the equations 4.1, 4.2, and 4.3 are derived.

KVL 1

$$V_{in} - L\frac{dI_L}{dt} = 0$$

$$\dot{x}_1 = \frac{dI_L}{dt} = \frac{V_{in}}{L} \tag{4.1}$$

KVL 2

$$V_C = -i_C R = -C\frac{dV_C}{dt}R$$

$$\dot{x}_2 = \frac{dV_C}{dt} = \frac{-V_C}{RC} \tag{4.2}$$

Output

$$V_o = -V_C \tag{4.3}$$

These equations can be written in state space form as shown in equation 4.4.

$$\begin{bmatrix}\dot{x}_1\\ \dot{x}_2\end{bmatrix} = \begin{bmatrix}\dot{I}_L\\ \dot{V}_C\end{bmatrix} = \begin{bmatrix}0 & 0\\ 0 & \frac{-1}{RC}\end{bmatrix}\begin{bmatrix}I_L\\ V_C\end{bmatrix} + \begin{bmatrix}\frac{1}{L}\\ 0\end{bmatrix} V_{in}$$

$$[y] = [V_o] = \begin{bmatrix}0 & -1\end{bmatrix}\begin{bmatrix}I_L\\ V_C\end{bmatrix} \tag{4.4}$$

For the off scenario, equations 4.5, 4.6, and 4.7 are obtained.

KVL 3

$$\frac{dI_L}{dt} = -\frac{V_C}{L}$$

KCL 1

$$I_L - C\frac{dV_C}{dt} - \frac{V_C}{R} = 0$$

Output

$$V_o = -V_C \tag{4.7}$$

$$\dot{x}_1 = \frac{dI_L}{dt} = -\frac{V_C}{L} \tag{4.5}$$

$$\dot{x}_2 = \frac{dV_C}{dt} = \frac{I_L}{C} - \frac{V_C}{RC} \tag{4.6}$$

In a similar manner, circuit equations are translated into state-space of the off mode as in equation 4.8.

$$\begin{bmatrix} \dot{x}_1 \\ \dot{x}_2 \end{bmatrix} = \begin{bmatrix} \dot{I}_L \\ \dot{V}_C \end{bmatrix} = \begin{bmatrix} 0 & -\frac{1}{L} \\ \frac{1}{C} & \frac{-1}{RC} \end{bmatrix} \begin{bmatrix} I_L \\ V_C \end{bmatrix} + \begin{bmatrix} 0 \\ 0 \end{bmatrix} V_{in}$$
$$\begin{bmatrix} y \end{bmatrix} = \begin{bmatrix} V_o \end{bmatrix} = \begin{bmatrix} 0 & -1 \end{bmatrix} \begin{bmatrix} I_L \\ V_C \end{bmatrix} \tag{4.8}$$

Averaged state-space model

With the two state-space models, an averaged version can be derived. The assumption required for applying this technique is that, given a switching frequency in the kilohertz range, there is no substantial variation in the system during a one switching cycle. In other words, operation from one switching cycle to the next is considered steady-state.

In this scenario, we define the total cycle of the buck-boost as $T = d + (1 - d) = d + \bar{d}$, where the two models contribute in varying degrees depending on the duty cycle, as show in equation 4.9

$$\text{Average}_{\text{ state-space}} = (\text{On mode}_{\text{ state-space}}) * d + (\text{Off mode}_{\text{ state-space}}) * \bar{d} \tag{4.9}$$

Once calculated the final model results in equation 4.10.

$$\begin{bmatrix} \dot{x}_1 \\ \dot{x}_2 \end{bmatrix} = \begin{bmatrix} \dot{I}_L \\ \dot{V}_C \end{bmatrix} = \begin{bmatrix} 0 & -\frac{\bar{d}}{L} \\ \frac{\bar{d}}{C} & \frac{-1}{RC} \end{bmatrix} \begin{bmatrix} I_L \\ V_C \end{bmatrix} + \begin{bmatrix} \frac{d}{L} \\ 0 \end{bmatrix} V_{in}$$
$$[y] = [V_o] = \begin{bmatrix} 0 & -1 \end{bmatrix} \begin{bmatrix} I_L \\ V_C \end{bmatrix} \tag{4.10}$$

Small-signal analysis

The state-space averaged model obtained still contains nonlinear properties, therefore the model must be further simplified. Small-signal analysis technique is widely used to approximate the behaviour. The assumption underlying is that deviations from the average operating point are small enough, allowing linearisation of equations. The technique starts with application of the perturbation theory. As shown in equations 4.11 the time-dependant variables are decomposed into steady-state and small-signal.

$$\begin{aligned} x &= X + \Delta x \\ y &= Y + \Delta y \\ \dot{x} &= \dot{X} + \Delta \dot{x} \\ d &= d + \Delta d \end{aligned} \tag{4.11}$$

When perturbing x, changes are introduces in other variables as in 4.12.

$$\begin{aligned} I_L &= I_L + \Delta i_L \\ V_C &= Vc + \Delta v_c \end{aligned} \tag{4.12}$$

Perturbation of y introduces the changes changes shown in 4.13.

$$\begin{aligned} V_o &= V_o + \Delta v_o \\ V_{in} &= V_{in} + \Delta v_{in} \end{aligned} \tag{4.13}$$

When perturbations are implemented in averaged matrices, the enlarged model shown in 4.14 is obtained.

$$\begin{bmatrix}\dot{X}_1+\Delta\dot{x}_1\\ \dot{X}_2+\Delta\dot{x}_2\end{bmatrix}=\begin{bmatrix}\dot{I}_L+\Delta\dot{i}_L\\ \dot{V}_C+\Delta\dot{v}_C\end{bmatrix}=\begin{bmatrix}0 & \frac{-\bar{d}+\Delta d}{L}\\ \frac{\bar{d}-\Delta d}{C} & \frac{-1}{RC}\end{bmatrix}\begin{bmatrix}I_L+\Delta i_L\\ V_C+\Delta v_C\end{bmatrix}+\begin{bmatrix}\frac{d+\Delta d}{L}\\ 0\end{bmatrix}(V_{in}+\Delta v_{in})$$

$$\begin{bmatrix}Y+\Delta y\end{bmatrix}=\begin{bmatrix}V_o+\Delta v_o\end{bmatrix}=\begin{bmatrix}0 & -1\end{bmatrix}\begin{bmatrix}I_L+\Delta i_L\\ V_C+\Delta v_C\end{bmatrix} \tag{4.14}$$

When the equations for each state are extracted and expanded as in equations 4.15 and 4.16, the small-signal components can be identified, as well as the quiescent and nonlinear elements.

$$\overbrace{\dot{I}_L}^{DC}+\overbrace{\Delta\dot{i}_L}^{Small\ signal}=\frac{\overbrace{-\bar{d}V_C+dV_{in}}^{DC}+\overbrace{\Delta dV_C-\bar{d}\Delta v_C+\Delta dV_{in}+d\Delta v_{in}}^{Small\ signal}+\overbrace{\Delta d\Delta v_C+\Delta d\Delta v_{in}}^{Nonlinear}}{L} \tag{4.15}$$

$$\overbrace{\dot{V}_C}^{DC}+\overbrace{\Delta\dot{v}_C}^{Small\ signal}=\frac{\overbrace{\bar{d}I_L}^{DC}-\overbrace{\Delta dI_L+\bar{d}\Delta i_L}^{Small\ signal}-\overbrace{\Delta d\Delta i_L}^{Nonlinear}}{C}-\frac{\overbrace{V_C}^{DC}}{RC}-\frac{\overbrace{\Delta v_C}^{Small\ signal}}{RC} \tag{4.16}$$

When only small signal is kept, the resulting equations reduce to 4.17 and 4.18.

$$\Delta\dot{i}_L=\frac{\Delta dV_C-\bar{d}\Delta v_C+\Delta dV_{in}+d\Delta v_{in}}{L} \tag{4.17}$$

$$\Delta\dot{v}_C=\frac{-\Delta dI_L+\bar{d}\Delta i_L}{C}-\frac{\Delta v_C}{RC} \tag{4.18}$$

Rearranging the formulas in 4.17 and 4.18 into state-state space as presented in equation 4.19, the A, B, C, and D matrices are obtained.

$$\begin{bmatrix}\Delta\dot{x}_1\\ \Delta\dot{x}_2\end{bmatrix} = \begin{bmatrix}\Delta\dot{i}_L\\ \Delta\dot{v}_C\end{bmatrix} = \overbrace{\begin{bmatrix}0 & -\frac{\bar{d}}{L}\\ \frac{\bar{d}}{C} & \frac{-1}{RC}\end{bmatrix}}^{A}\begin{bmatrix}\Delta i_L\\ \Delta v_C\end{bmatrix} + \overbrace{\begin{bmatrix}\frac{V_{in}+V_C}{L}\\ \frac{-I_L}{C}\end{bmatrix}}^{B_1}[\Delta d] + \overbrace{\begin{bmatrix}\frac{d}{L}\\ 0\end{bmatrix}}^{B_2}[\Delta v_{in}] \tag{4.19}$$

$$[\Delta y] = [\Delta v_o] = \overbrace{\begin{bmatrix}0 & -1\end{bmatrix}}^{C}\begin{bmatrix}\Delta i_L\\ \Delta v_C\end{bmatrix}$$

The feedforward input from source is not present in the system, therefore matrix D = 0. With the matrices defined, the Laplace formula in 4.20 for transforming state-space to transfer function can be used. As the interest of the application is to end up with a transfer function which is Single Input Single Output (SISO), it is required to define which input matrix is kept. As the parameter to be controlled is the duty cycle, matrix B_1 is kept, during the transformation.

$$\frac{y(s)}{u(s)} = C \cdot (sI - A)^{-1} \cdot B_1 \tag{4.20}$$

The resulting transfer function is shown in equation 4.21.

$$H(s) = \frac{\Delta v_o(s)}{\Delta d(s)} = \frac{\frac{V_o \bar{d} R}{d} - \frac{V_o L s}{\bar{d}}}{RLCs^2 + Ls + \bar{d}^2 R} \tag{4.21}$$

4.2 Analysis of the buck-boost converter model

4.2.1 Model settings and transfer function

Applying the model to a use case requires settings specific values for the output voltage, inductance, capacitance, resistance and duty cycle. This section explains what these values were set to and the reasoning for these decisions.

- **f**: The frequency is set to 62,5 kHz. This is due to PWM pin on the Arduino Uno being constrained to this as the maximum frequency setting, which is used in the physical implementation of the converter in Section 5.1.

- **R**: The internal resistance of a 96-series 86-parallel battery pack is estimated to be 9.8 Ω at 75% state of charge [45].
- **d**: The duty cycle and it's complement $\bar{d}$ are set to 0,5.
- **L**: The inductor value is calculated with Equation (4.22)[46]. A multiplier of 1,25 is used to surpass the minimum required limit for Continuous Conduction Mode.

$$L_{min} = 1,25 \cdot \frac{(\bar{d})^2 \cdot R}{2 \cdot f} = 2,45 \cdot 10^{-5} H \tag{4.22}$$

- **C**: The capacitor value is calculated with Equation (4.23)[46]. A multiplier of 1,25 is used again to surpass the minimal required limit for maintaining the desired ripple voltage. The ripple percentage $\frac{\Delta V_o}{V_o}$ is set to 1%.

$$C = 1,25 \cdot \frac{d}{\frac{\Delta V_o}{V_o} \cdot R \cdot f} = 1,0204 \cdot 10^{-4} F \tag{4.23}$$

- V_o: The output voltage is set to 350V, as that is the maximum voltage the chosen battery sizing can hold, as mentioned in Section 3.4.

The transfer function using the aforementioned values is defined as:

$$H(s) = \frac{-0,008575s + 1715}{1,22510^{-8}s^2 + 1,22510^{-5}s + 1,225} \tag{4.24}$$

4.2.2 Transfer function analysis

To control the buck-boost converter, it is necessary that a control loop is designed. In order to do so, the transfer function needs to be analysed for its characteristics.

Open loop

- $Zero = 200000$
- $Pole = -0.5 + 9.9875i$
- $Pole = -0.5 - 9.9875i$

Due to the right half plane zero, the system is a non-minimum phase system. With the poles on the left half lane the open loop system is stable with some oscillations due to a damping ratio less than 1. This can be observed in the open loop response plotted in Figure 4.4.

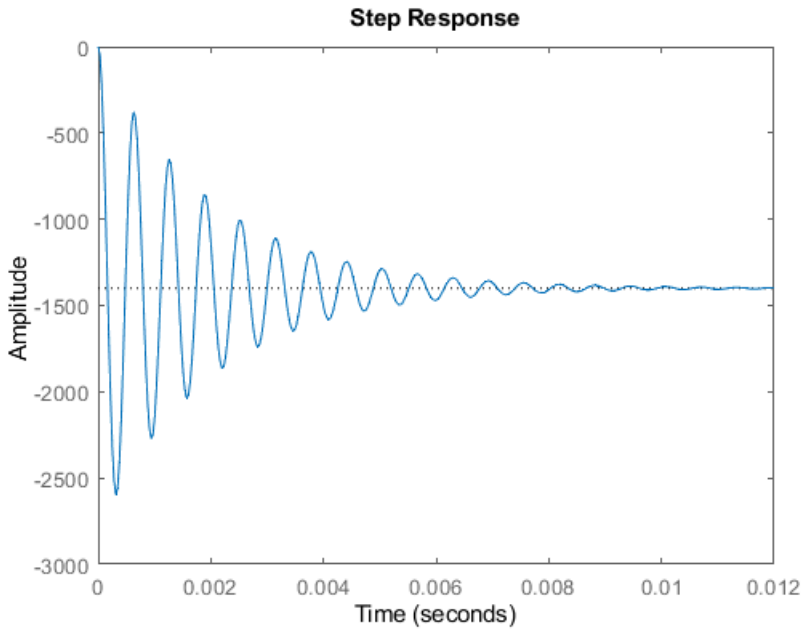

Figure 4.4: The open loop step response of the model of the buck-boost converter.

Closed loop

Observing the root locus plot for the function in Figure 4.5, it can be seen that very small gains up to around 0.00071 will raise the damping ratio to 1, however any higher gains will cause the system to become unstable due to one of the poles moving over to the right half plane.

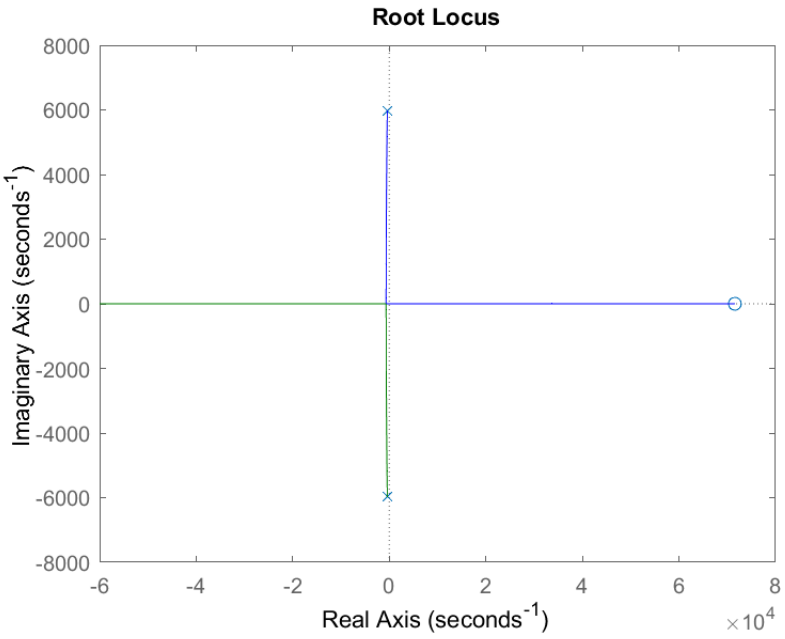

Figure 4.5: Root Locus plot of the transfer function.

Thus the closed loop system with unity gain is unstable.

4.3 Control of the system

Continuous control techniques are used to tune the controller, after which it is converted into a digital controller. The goals of the control are the following:

- Less than 1% overshoot
- A settling time of less than 1 second
- Steady state error of less than 1%
- Ripple voltage of less than 1%

4.3.1 Continuous controller

With the use of the Matlab PID Tuner Application and subsequent manual tuning, the control was found to fulfil the requirements set using only integral control. The integral value was set to -0,30907, giving the controller the function as per equation 4.25.

$$G(s) = \frac{-0.30907}{s} \tag{4.25}$$

Figure 4.6 shows the difference between applying I and PI control for the system, both at equal I values, with the P value at -0,0001. A variety of different P and I values were tried with no improvement in response, only insofar as P tended toward zero.

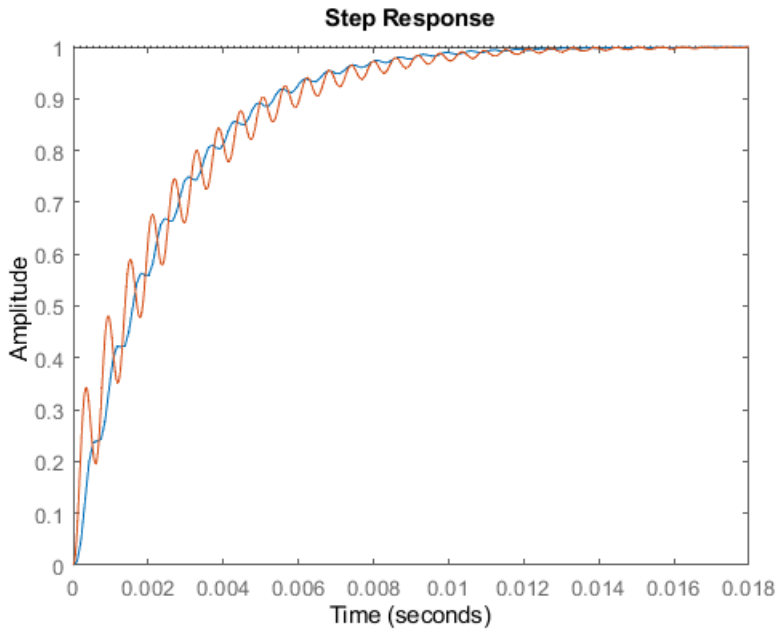

Figure 4.6: A step response showing the difference between I (blue) and PI (orange) control for the buck-boost model.

The resulting equation describing the system with implemented I-controller is shown in equation 4.26

$$H(s) \cdot G(s) = \frac{-0.00386s + 276.3}{1.70810^{-8}s^3 + 1.415 \cdot 10^{-5}s^2 + 0.6073s + 276.3} \tag{4.26}$$

4.3.2 Discrete controller

To translate the continuous controller to a digital one, Zero-Order-Hold discretization method was chosen as it models the digital to analog conversion found in a micro-controller. The sampling frequency chosen was 5 times that of the bandwidth of the system, giving some margin to the Nyquist frequency. The bandwidth of the system is $2,4699 \cdot 10^3$ Hz, so

the sampling period T_s is set to $1/(1,2349 \cdot 10^4)$ s. Using the Matlab function 'c2d' with these parameters, the Z-domain system in Equation (4.27) is derived.

$$H_z = \frac{0,002978z^2 + 0,01379z + 0,004124}{z^3 - 2,317z^2 + 2,26z - 0,9222} \tag{4.27}$$

The system step response is given in 4.7.

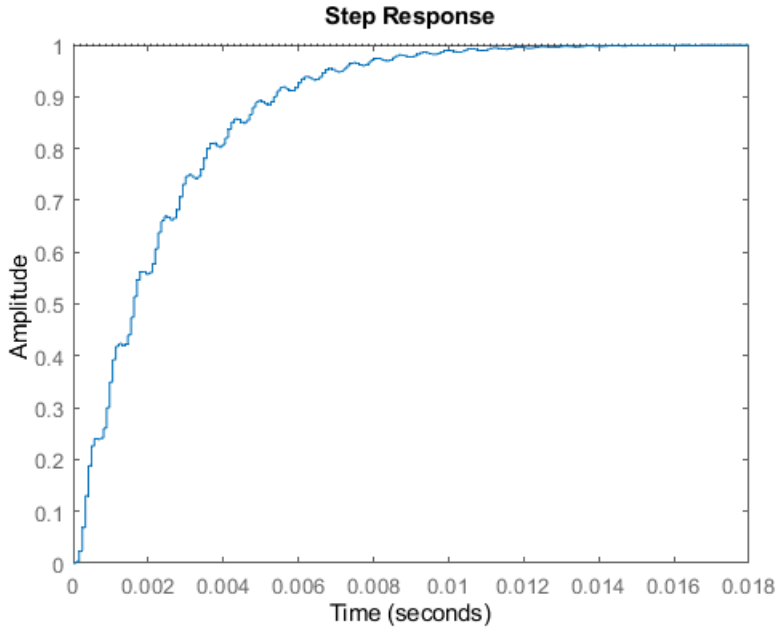

Figure 4.7: The step response of the combined digital controller, ZOH and plant.

The digitised system model fulfills the set requirements for settling time, steady state error, overshoot and ripple.

4.3.3 ADC model

Having modelled the DAC conversion with ZOH, it is also important to model the Analog-to-Digital conversion(ADC) which is present in the feedback loop of a digital control system. It is thus possible to model the frequency with which the ADC takes a measurement, and the accuracy with which it is measured. This is done using the Sample and Hold block and Quantizer block present in Simulink, as seen in figure 4.8.

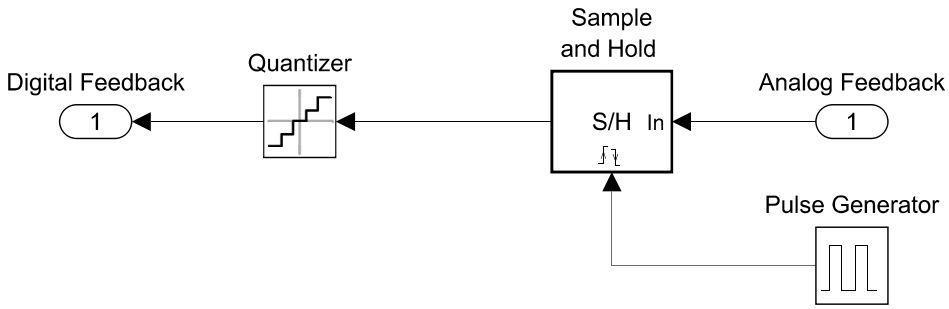

Figure 4.8: An overview of the ADC model in Simulink.

The Sample and Hold blocks model the sampling time of the controller, whereby for each pulse from the pulse generator it reads and holds a voltage value. The pulse generator being set to output a pulse at the chosen frequency of $7,3867 \cdot 10^3$ Hz. The Quantizer block models the 10 bit ADC accuracy, storing the read voltage in a 10 bit number.

4.4 Simulation

This section showcases the individual simulation results for the rectifier and buck-boost converter, as well as a simulation of them combined. All simulations are simulated in Simulink.

4.4.1 Rectifier

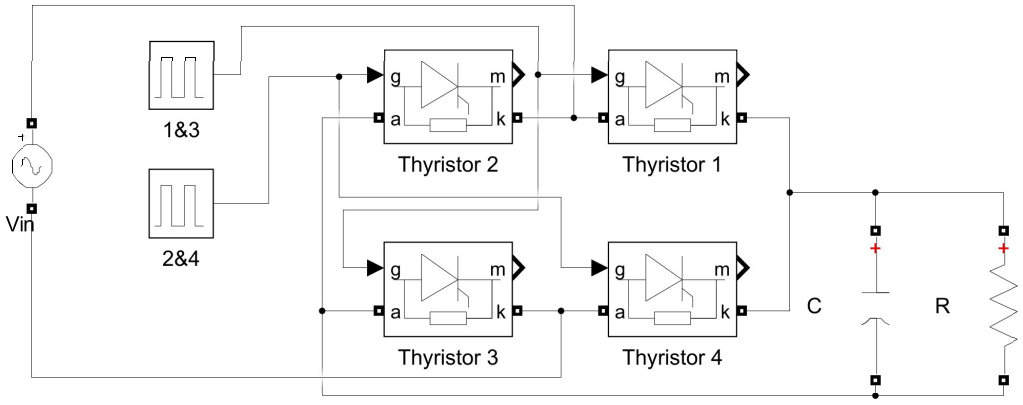

Figure 4.9: An overview of the rectifier circuit.

The rectifier circuit shown in 4.9 is based on the circuit architecture called a controlled full-wave rectifier[46]. This type of rectifier works by alternatingly switching thyristors at 180°phase difference. When the AC input is positive, thyristors 1&3 are open, and when the AC input is negative thyristors 2&4 conduct, flipping the whole sine wave period, therefore called full wave. This active rectifier can be used for bucking voltage output by varying the firing angle of the thyristors between 0 and 90 degrees. Moreover, it is also capable of functioning as an inverter. This could be useful for future development of the BESS system where battery to grid direction is concerned. However, as the buck-boost is used in this project for voltage control to the battery side, the thyristor firing angle is set to 0 degrees, effectively making it a passive rectifier. Since the output of the rectifier is not constant, a capacitor is applied in parallel to the load, smoothing the output. To calculate the required capacitor value, equation 4.28 is used. Simulation showed that a slightly higher value gave a better result, thus the value was multiplied by 2.

$$C_{filter} = 2 \cdot \frac{1}{2 \cdot f \cdot R \cdot \frac{\Delta V_o}{V_m}} = 2 \cdot \frac{1}{2 \cdot 50Hz \cdot 9,8\Omega \cdot 0,01} = 0,204F \tag{4.28}$$

This output is smoothed out with a capacitor. The impact of the thyristor switching and capacitor in the rectifier circuit with a 230V AC input is shown in figure 4.10.

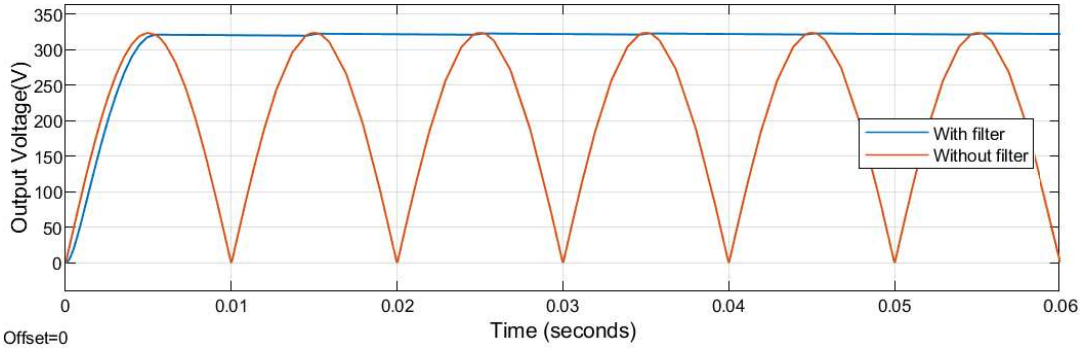

Figure 4.10: A plot showing the impact of the thyristor switching on the AC input (orange) and the impact of the capacitor on the output voltage(blue).

4.4.2 Buck-boost converter

This simulation aims to test the buck-boost converter separately in order to verify that the derived controller works as intended. The circuit structure and connected control loop is shown in figure 4.11.

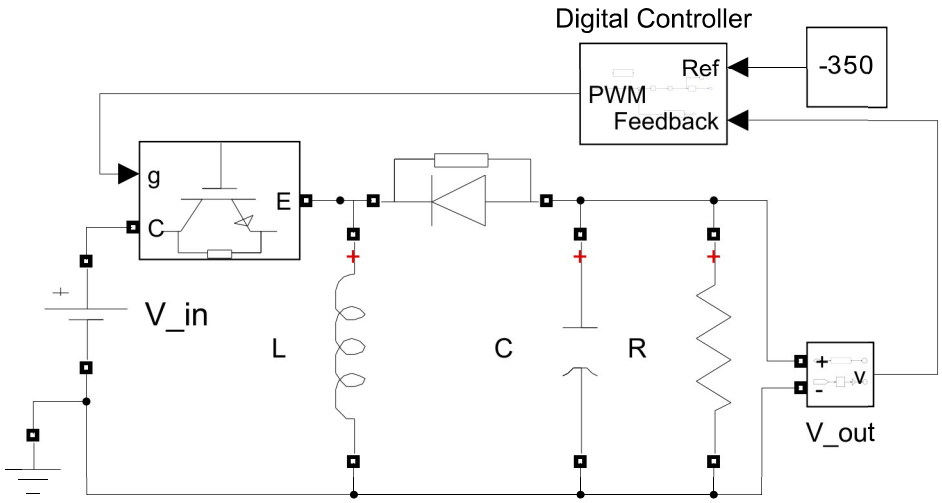

Figure 4.11: A Simulink diagram of the buck-boost converter circuit with the controller.

Using the values for components in Section 4.2 and controller as described in Section 4.3, the buck-boost converter was simulated in both modes of operation, boosting the 230V input to -350V, and bucking the 350V input to -230V. The output voltages of these simulations are shown in figure 4.12

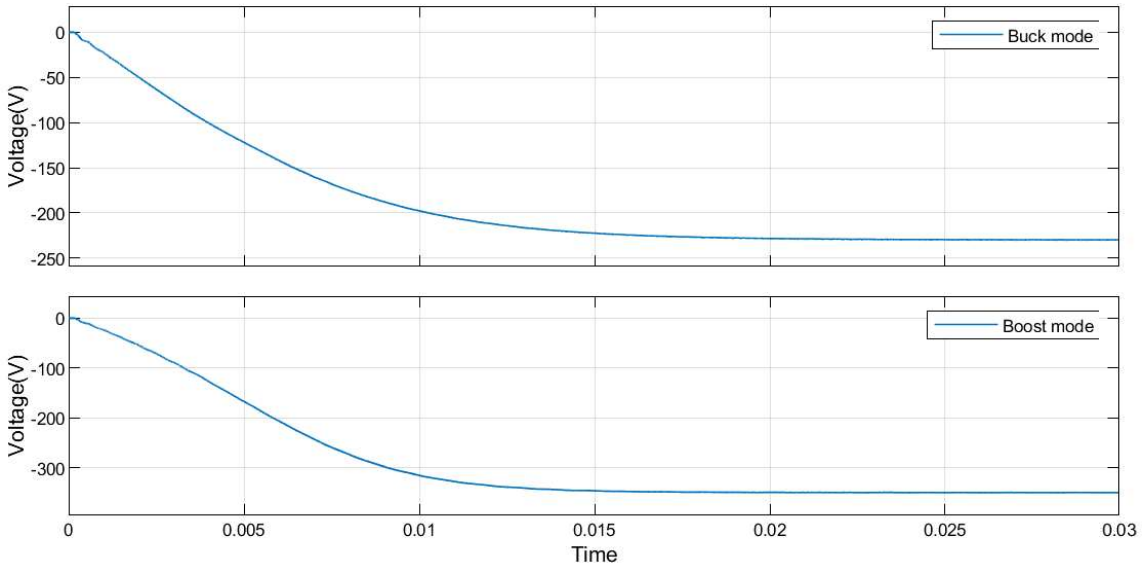

Figure 4.12: Results from simulating the buck-boost circuit with the controller in both buck and boost mode.

The results fulfil the set requirements for the controller in both bucking and boosting mode of operation.

4.4.3 Rectifier and buck-boost converter

Furthermore, the rectifier and the buck-boost models were tested together, connected as shown in Figure 4.13.

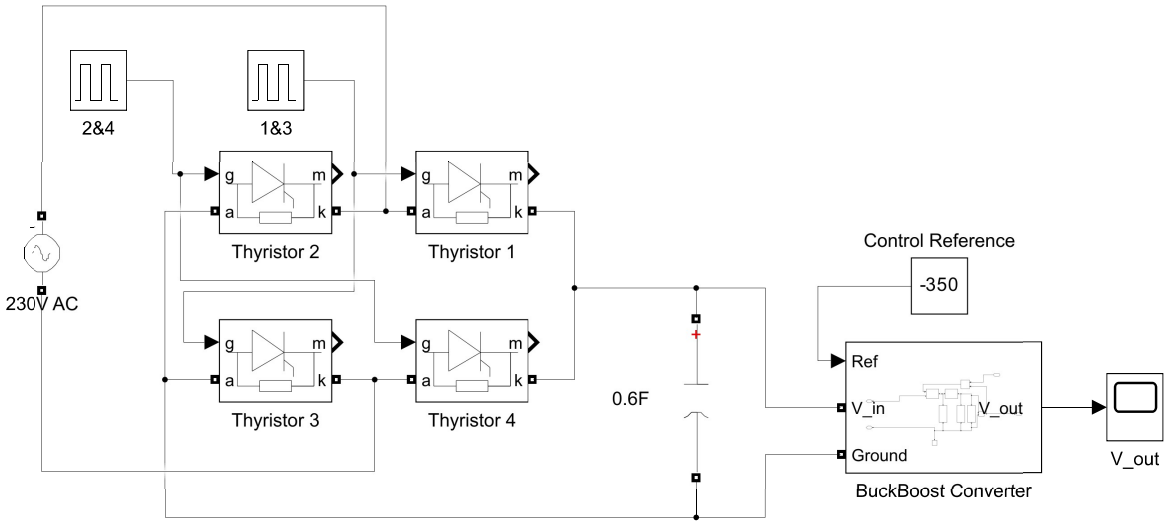

Figure 4.13: An overview of the rectifier and buck-boost converter circuit.

Testing the rectifier circuit connected to the buck-boost converter circuit together with 230VAC input and -350VDC output reference for the controller, the results were as given in figure 4.14.

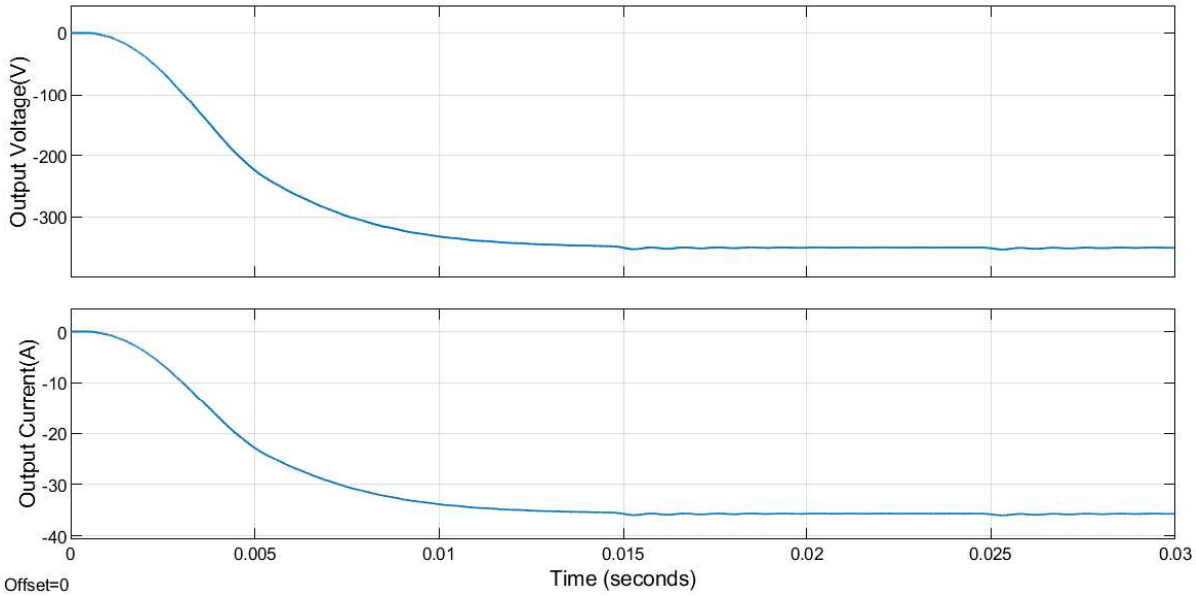

Figure 4.14: Plots showing the buck-boost converters input current and output voltage.

Observing the output voltage, it contains a ripple of between 2V-5V, which is slightly above the set goal. However, the output has no overshoot, settles in less than 1 second and is within the steady state error limit.

Chapter 5

Prototype Design, Testing and Validation

In this chapter, laboratory implementation of a part of the model from Figure 2.1 is described. A buck-boost converter is built on a breadboard and the prototype is then tested.

5.1 Implementation

Although all parts of the BESS discussed in Section 2.1 are vital for the function of it, a decision was made to physically implement one subsystem because of limitations introduced in Section 2.3. The subsystem that was built is the buck-boost converter as its components were readily available at the laboratory and its implementation was considered a good learning opportunity.

5.1.1 Prototype design

The prototype circuit consists of four sections: a micro-controller, a MOSFET gate driver block, a buck-boost converter block and an inverting operational amplifier block, as illustrated by the diagram in Figure 5.1.

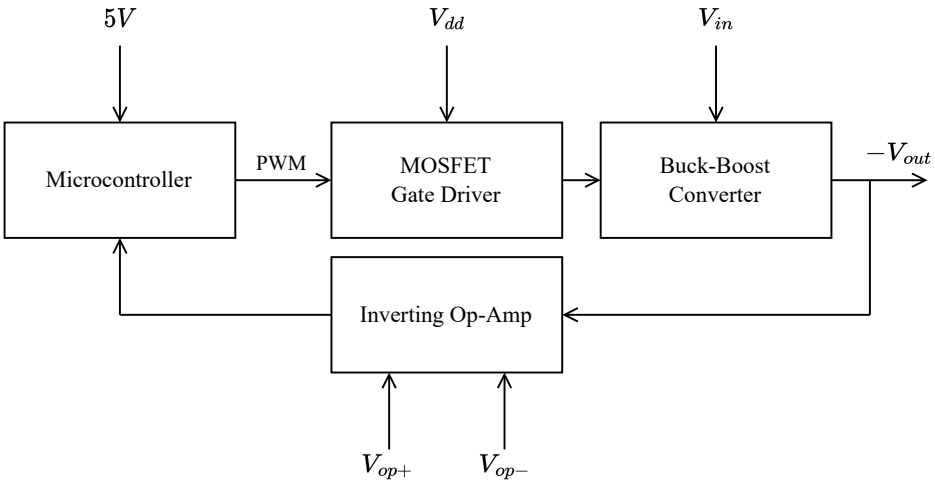

Figure 5.1: Block diagram of the prototype.

To turn an N-channel MOSFET on, a gate-to-source voltage has to be sufficiently high [46]. The $5V$ logic-level signal of Arduino UNO, which is used to control the circuit, would be suitable to operate a MOSFET for low side switching, where source is connected to common ground, thus at a lower potential than gate. However, the position of the switch in a buck-boost converter requires that high side of the circuit is switched, as shown in Figure 4.2. Omitting a voltage drop on MOSFET, the voltage on its source is virtually the same as the input voltage V_{in} applied to drain, which is above $5V$. With source at a higher potential than the logic-level signal it is not possible to control the MOSFET with Arduino directly, and a MOSFET gate driver in combination with a bootstrap circuit is needed[47]. This circuit creates a higher gate-to-source voltage and thus allows Arduino to control the MOSFET.

The implemented buck-boost converter outputs negative voltage, which is not possible to measure with Arduino directly. Therefore, an operational amplifier in inverting configuration was used in the feedback loop.

To operate the circuit it was decided to use V_{in} of $10V$ at the input of the buck-boost converter and following the specifications of the MOSFET driver V_{dd} of $15V$ to power the driver circuit[48]. The operational amplifier is powered by $V_{op} = \pm 18V$ [49]. Connections of all components are illustrated in a circuit diagram in Figure 5.2.

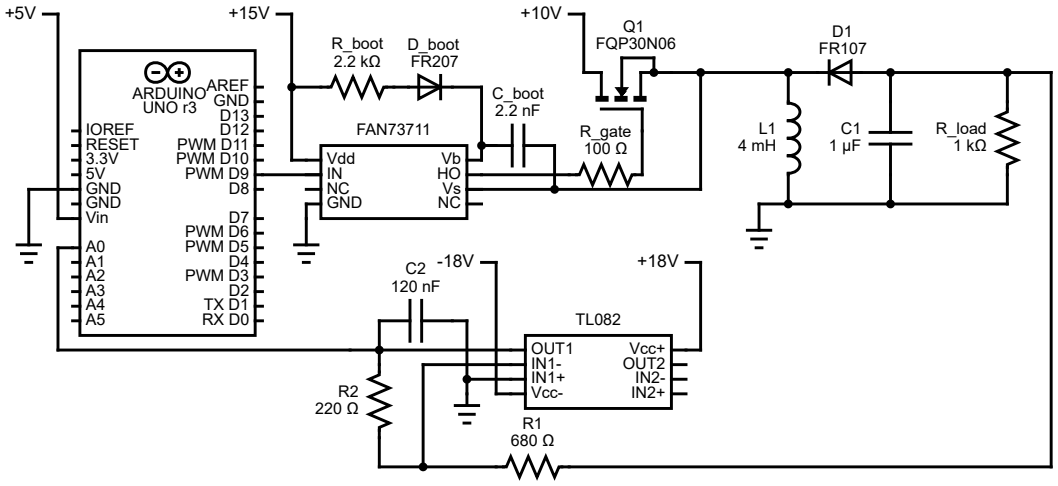

Figure 5.2: Circuit diagram of the prototype.

Buck-boost converter

Because industrial DC-DC converters usually operate at high switching frequencies of up to 1 MHz[50], it was decided to operate the buck-boost converter at the highest PWM output frequency possible on the Arduino, 62,5kHz. It was decided to test the buck-boost converter in a range of -5V to -15V, and thus the capacitor and inductor values were calculated with the duty cycle that would give the larger value. Thus for the inductor the value was calculated with duty cycle in Equation (5.1) and the capacitor with the duty cycle in Equation (5.2). The load was set to $R_{load} = 1k\Omega$.

$$D = \frac{|V_o|}{V_{cc} + |V_o|} = \frac{5}{10+5} = \frac{1}{3} \approx 33\% \tag{5.1}$$

$$D = \frac{|V_o|}{V_{cc} + |V_o|} = \frac{15}{10+15} = 60\% \tag{5.2}$$

Furthermore, the minimum inductance of the coil was calculated using Equation (5.3).

$$L_{min} = \frac{(1-D)^2 \cdot R}{2f} = \frac{(1-0,33)^2 \cdot 1000}{2 \cdot 62,5 \cdot 10^3} = 3,6mH \tag{5.3}$$

The chosen coil was selected from the inventory of the laboratory with an inductance of $L = 4mH$. Moreover, to limit the voltage ripple to 1%, capacitance of the output capacitor was calculated as shown in Equation (5.4).

$$C = \frac{|V_o| \cdot D}{\Delta V_o \cdot r \cdot f} = \frac{5 \cdot 0,6}{0,05 \cdot 100 \cdot 62,5 \cdot 10^3} = 0.96\mu F \tag{5.4}$$

The capacitor value available that was used in the circuit was 1µF.

MOSFET gate driver

The driver utilised in the prototype is based on FAN73711 integrated circuit (IC) and it was implemented according to the typical application diagram from the datasheet[48], including the boostrap resistor, diode, and capacitor, as well as the bootstrap gate resistor. The values of these components were calculated following the application note by the manufacturer [51]. The employed switch for the buck-boost circuit is the N-channel MOSFET FQP30N06L [52], because of its sufficient drain-source voltage (V_{DDS}) of 60V, Drain Current (I_D) of 32A, and delay times that allow for up to 5.88MHz switching ($f_{Max} = (t_{d(on)} + t_{d(off)})^{-1} = (40nS + 120nS)^{-1} = 5.88MHz$). For the boostrap diode the requirements were a Maximum Recurrent Peak Reverse Voltage (VRRM) larger than V_{in} and a quick recovery time to minimize the feedback from the bootstrap capacitor to the power supply. The chosen diode is the FR207[53] with a VRRM of 1000V and a recovery time of 500 nS. Calculation of the bootstrap capacitor C_{boot} depends on characteristics of the gate driver, the boostrap diode, and the MOSFET, as defined by equation 5.5.

$$C_{boot} = \frac{Q_{total}}{\Delta V_{boot}}$$

$$Q_{total} = Q_{gate} + (I_{lkcap} + I_{lkgs} + I_{qbs} + I_{lk} + I_{lkdiode}) \cdot \frac{D}{f} + Q_{ls}$$

$$\Delta V_{boot} = V_{dd} - V_f - V_{gs} \tag{5.5}$$

Extracting the values from the datasheets [53][52][48], the value of the capacitor can be determined, as in 5.6, where 1/3 or approximately 33% is the duty cycle for bucking.

$$Q_{total} = 2 \cdot 10^{-8} + (0 + 10^{-7} + 12 \cdot 10^{-5} + 10^{-5} + 5 \cdot 10^{-6}) \cdot \frac{1/3}{62500} + 3 \cdot 10^{-9} = 2.37 \cdot 10^{-8} C$$

$$\Delta V_{boot} = 15 - 1.2 - 1 = 12.8V$$

$$C_{boot} = \frac{2.37 \cdot 10^{-8}}{12.8} = 1.85nF \tag{5.6}$$

In the same way, when boosting, using a duty cycle of 60% the required capacitor was $1.90nF$, thus the closest available value of 2.2nF was chosen.

The function of the bootstrap resistor R_{boot} is to reduce peak currents at the bootstrap diode during its start-up phase [54]. In the prototype, an undesired behaviour was detected. A voltage built up at the gate before the rising edge of the PWM pulse as shown in Figure Figure 5.3(a), as well as slow response to the falling edge. This undesired behaviour was partially controlled by increasing the value of R_{boot} to $2.2k\Omega$ as depicted in Figure 5.3(b).

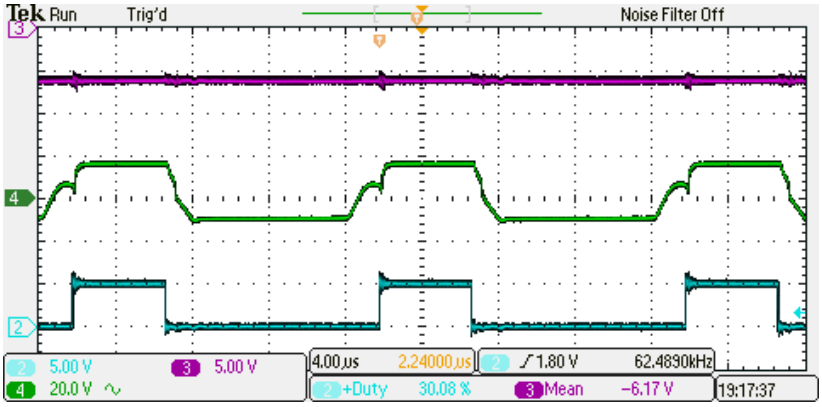

(a) No bootstrap resistor used.

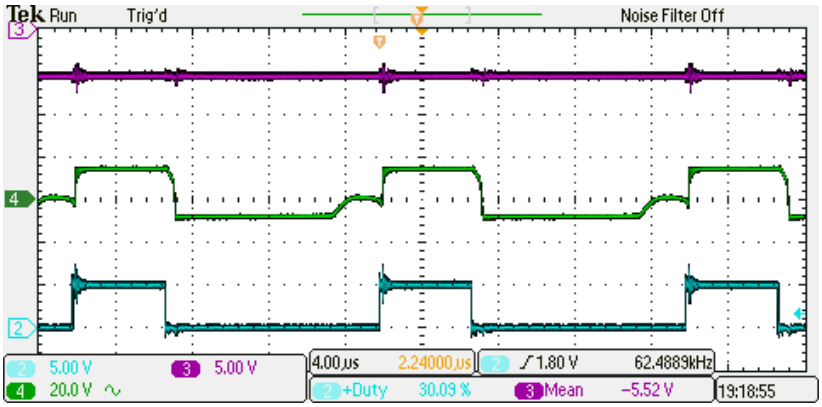

(b) Bootstrap resistor $R_{boot} = 2.2k\Omega$ used.

Figure 5.3: Showing the effect of a bootstrap resistor on the gate driver output. Channel 2 (cyan): Arduino PWM pulse. Channel 4 (green): MOSFET Gate voltage without (a), and with (b) a bootsrap resistor.

The gate resistor R_{gate} was selected empirically. The objective was to avoid a too low resistance value, which allows gate ringing on the gate signal, or a too high resistance value, which over-damps the signals and extends the switching times unnecessarily [55]. The optimal value was determined by observing the gate signal response on an oscilloscope [56]. A R_{gate} of 100Ω produced a response between critically damped and underdamped.

Operational amplifier

As previously mentioned, output voltage V_{out} of the buck-boost converter is negative, which makes it impossible to measure it by Arduino directly. Therefore, an op-amp in inverting mode of operation was placed in the feedback loop to create a positive voltage proportionally large to V_{out}. At a maximum of -15V output of the converter, the voltage is scaled by resistors $R1 = 670$ and $R2 = 220$, such that the maximum voltage read by the Arduino was $(220/670) \cdot 15V = 4,93V$. Filtering capacitor C2 was used to remove noise which was initially observed in the measured signal. With later rearrangement of the circuit on the breadboard the noise was no longer present, but it was decided to keep the capacitor in place nonetheless.

Implementation on breadboard

Based on calculations and design decisions from previous sections, the circuit was implemented on a breadboard, which is shown in Figure 5.4.

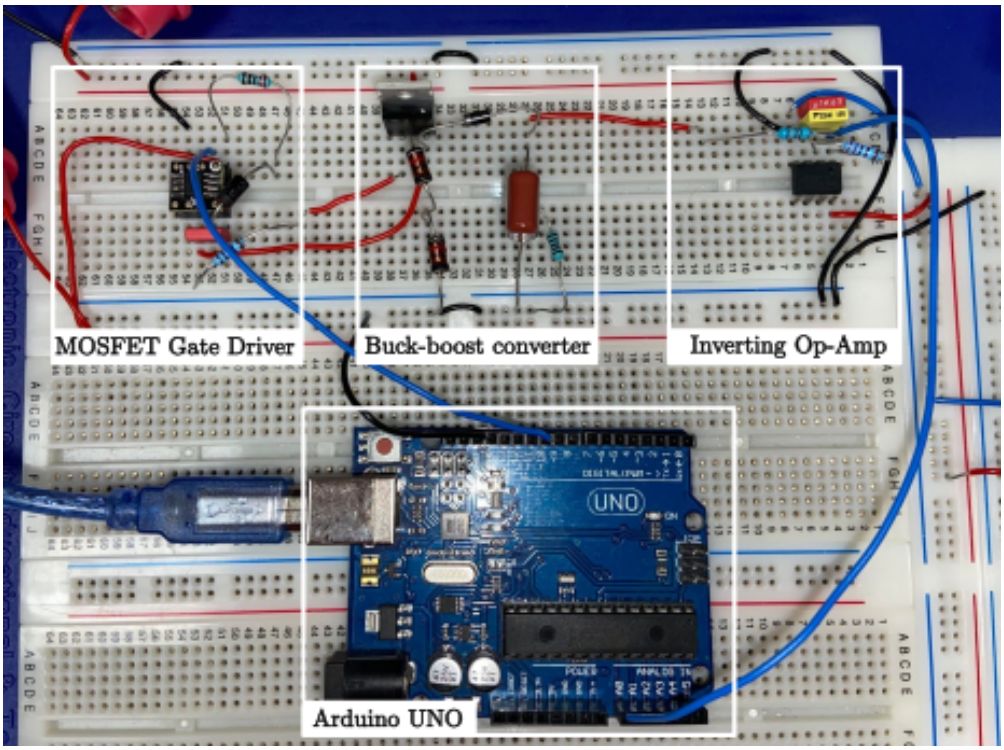

Figure 5.4: Picture of the laboratory setup of the Arduino controlled buck-boost converter.

5.1.2 Arduino Code

Implementing the control loop was done via programming the Arduino using the library called pid_v1_bc[57]. The controller was tuned in Matlab using the physically implemented circuit values in Section 5.1. The new controller values were then implemented in the code for the Arduino, which can be found in Appendix B. The Matlab code for deriving the lab-sized model for controller tuning can be found in Appendix A. An issue that was discovered during programming was that the PID library was unable to handle negative controller values. This was remedied by inverting all controller values, voltages and setpoints to positive ones in the code, giving the same control output.

5.2 Testing and validation

After the prototype circuit was built, it was tested to verify the functionality of the controller. Moreover, efficiency of the DC-DC converter was measured.

5.2.1 Control loop test

The first experiment conducted was to test whether or not the simulated control loop would function when implemented in the physical model. Testing was done by changing the setpoint in the code from -5 to -15 at intervals of 2. The resulting responses in the circuit for the varying setpoints can be seen in Figure 5.5.

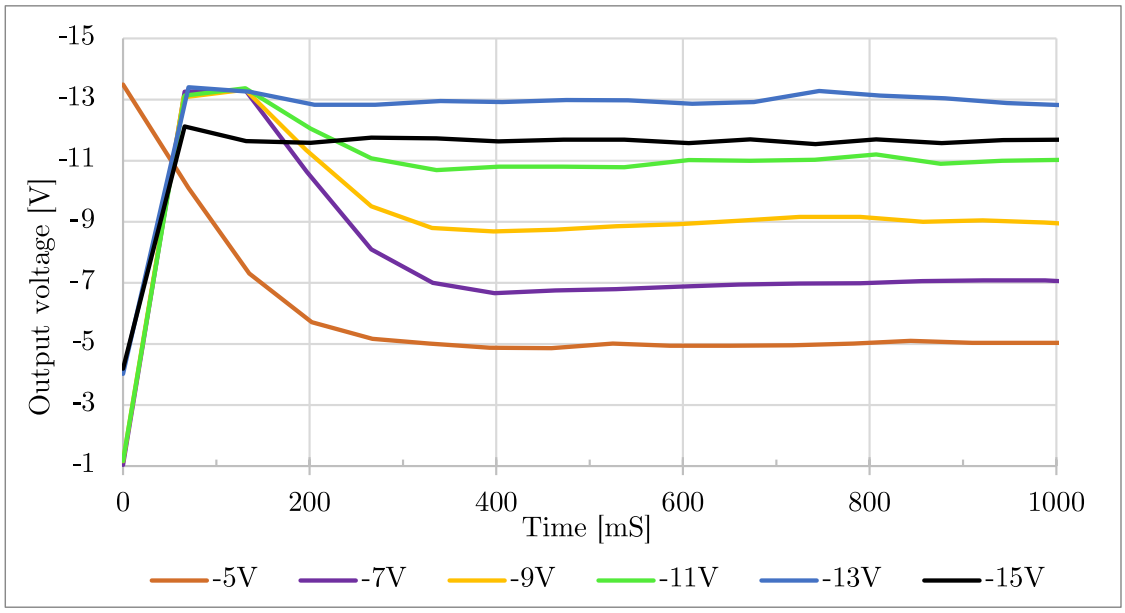

Figure 5.5: Step response of the controller for the buck-boost at different reference voltages.

Table 5.1: Showcasing the average and ripple voltage results from the controller testing.

Reference (V)	Average (V)	Max 90% (V)	Min 10% (V)	Ripple (V)	Ripple (%)
-5	-5,00	-5,10	-4,94	0,16	3,2%
-7	-6,99	-7,09	-6,87	0,22	3,1%
-9	-9,00	-9,12	-8,92	0,20	2,2%
-11	-11,00	-11,14	-10,87	0,27	2,5%
-13	-13,01	-13,12	-12,86	0,26	2,0%
-15	-11,60	-11,69	-11,51	0,18	1,6%

The ripple voltage in Table 5.1 is calculated by taking a set of samples once the signal is settled and subtracting the minimum from the maximum. Top and bottom 10% are excluded to eliminate potential false readings from the microcontroller.

Comparing the laboratory results to the initial controller goals set in Section 4.2, the outcome was as follows:

- **Less than 1% overshoot**: This was not achieved, as can be observed that most setpoints first rose to around -13V before settling.
- **A settling time of less than 1 second**: This was achieved for all setpoints.

- **Steady state error of less than 1%**: In Table 5.1 the average voltage for all except the -15V setpoint are within 1% of the setpoint.
- **Ripple voltage of less than 1%** The ripple voltage shown in Table 5.1 varied between 1,6% and 3,2%, not achieving the set goal.

It can be seen that the controller in the test demonstrated in Figure 5.5 is not able to run the circuit at a setpoint of -15V, as its output is around -11,6 V. The hypothesis is that the op-amp is at fault, and unable to operate with an input signal of such magnitude and skewing the voltage readings, despite its specifications stating capability of taking input signals as high as $\pm$15 V. The buck-boost circuit itself is able to operate at above -15 V as demonstrated in Section 5.2.2.

5.2.2 Efficiency measurement

Because it would be reasonable to measure efficiency on a system considered earlier in Section 3.4, it was decided to exercise this measurement on the prototype to provide data for economical analysis. Efficiency for electrical circuits is defined as useful power output divided by the power input, this can be derived from Ohm's Law as shown in Equation (5.7).

$$\eta = \frac{P_{in}}{P_{out}} = \frac{V_{in} \cdot I_{in}}{V_{out} \cdot I_{out}} \tag{5.7}$$

Industrial DC-DC converters operate at high frequencies in hundreds of kilohertz up to 1MHz to lower the required values of inductance and capacitance while improving converter dynamics, however at the cost of decreased efficiency[50]. Because the highest possible switching frequency of Arduino, 62,5 kHz, was considered slow compared to industrial standards, it was decided to test the converter at a frequency twice as fast, 125 kHz, using a function generator and downsizing the coil and the capacitor according to 4.22 and 4.23. This test proved unsuccessful as the circuit failed to operate and output any voltage. Subsequently, it was decided to compare the performance of the converter operating at half of the initially set frequency, 31,25 kHz.

The test consisted of calculating the efficiency of the buck-boost converter by measuring the input and output power using volt- and ampere-meters for duty cycles between 20% and 70%, thus in both modes of operation. A function generator was used as a PWM signal input in place of the Arduino control circuit, running the first set of measurements at 62,5 kHz and the second set at 31,25 kHz. The results of these measurements are shown in Table 5.2.

The measurements proved that lowering the switching frequency has a positive impact on efficiency of the converter, with the lower switching frequency yielding 64% efficiency

Table 5.2: Measured efficiency and output voltage for input voltage $V_{in} = 10V$ and switching frequency of 62,5 kHz and 31,25 kHz.

$Duty\ cycle(\%)$	$P_{in}(mW)$	$P_{out}(mW)$	$\eta(\%)$	$V_{out}(V)$
70	525,1	238,2	45	15,4
65	361,1	183,5	51	13,5
60	253,4	137,2	54	11,7
55	181,0	101,3	56	10,0
50	130,9	73,85	56	8,58
45	95,03	53,00	56	7,27
40	68,30	37,06	54	6,08
35	48,10	24,95	52	4,99
30	32,52	15,69	48	3,96
25	20,42	8,71	43	2,95
20	10,90	3,61	33	1,90

(a) Switching frequency of 62,5 kHz.

$Duty\ cycle(\%)$	$P_{in}(mW)$	$P_{out}(mW)$	$\eta(\%)$	$V_{out}(V)$
70	446,6	242,6	54	15,6
65	305,1	179,5	59	13,4
60	213,7	132,0	62	11,5
55	151,7	96,49	64	9,81
50	108,2	69,98	65	8,36
45	77,32	50,44	65	7,10
40	65,60	43,02	66	6,55
35	61,43	40,08	65	6,33
30	40,88	25,50	62	5,05
25	26,46	15,94	60	3,99
20	15,89	8,63	54	2,94

(b) Switching frequency of 31,25 kHz.

on average when operating between 30% and 60% duty cycle. This fact would benefit the economical aspect of the BESS considered in this report. A visual comparison of the measured data is provided in Figure 5.6.

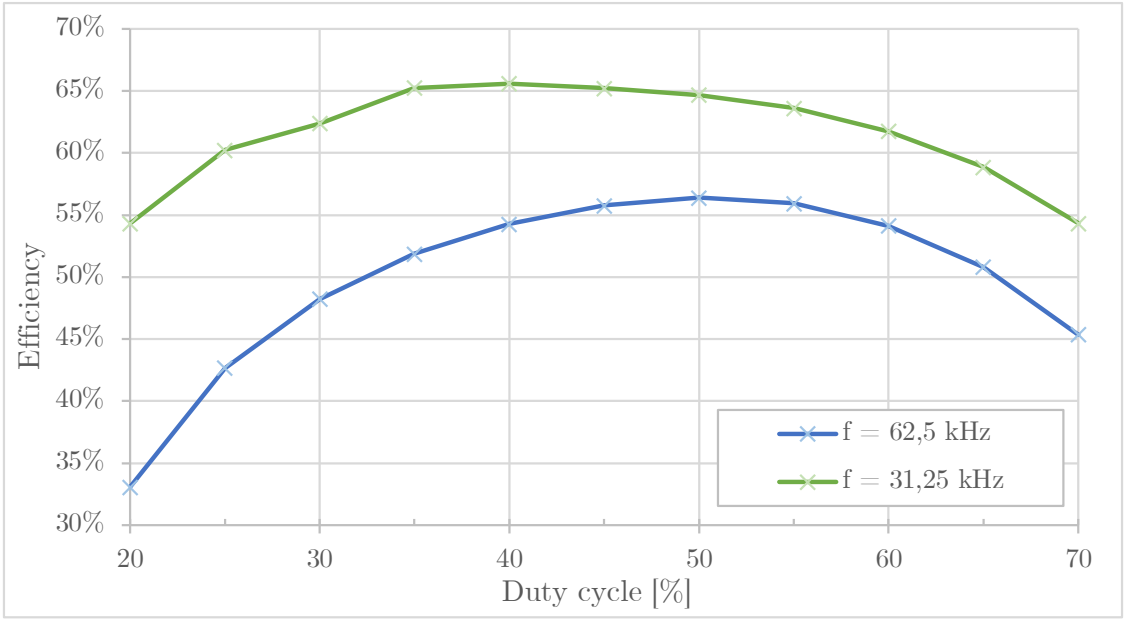

Figure 5.6: Chart showing the relation of efficiency to switching frequency at different duty cycles.

Chapter 6

Discussion and Conclusion

6.1 Discussion

During the course of the project several issues and areas of improvement were identified. The following chapter discusses some of these and their potential solutions, were this project to be further developed.

One of the larger issues encountered was that of the negative voltage output of the Buck-Boost converter. This would have several undesirable implications when implementing the system. Charging the batteries would not be possible unless the terminals were connected in reverse. However this would present an issue if reversing power direction of the system. During the implementation of the controller, measurement issues due to the negative output occurred. These were remedied by inverting and scaling the output with an operational amplifier for the microcontroller to be able to process it with its ADC. For future applications, it would be beneficial to work with converter circuits which are non-inverting, such as a SEPIC converter, although for the scope of the project it was not considered because of its higher complexity for modelling and control.

In the best case economic scenario, not taking efficiency into account, the payback time was found to be around 7,66 years. With the batteries dimensioned to function for the full 5 hours window this would mean around 2 years of profit. Should the batteries function well beyond this it could add to the profitability. For the high payback case of 31,4 years it would not be beneficial from an economic point of view. Additionally, the efficiency of the system will impact the economics greatly. Buck-boost converters are in principle able to achieve efficiencies around 95%[58]. The lab prototype built did not achieve such levels of efficiency, which if scaled linearly would greatly impact the potential payback time of the system. At the current maximum achieved efficiency of 64%, the payback time would scale to between 12,3 and 49,1 years. Improving efficiency would thus be of high importance to

future work within the area for this to be an economically viable venture. As mentioned in 3.4, tax incentives could be one way in which this type of solution could become more cost competitive. The tendency for technology costs to lower over time could also impact the payback time in a positive way.

One of the factors which affected the efficiency here was the switching frequency. Although the switching frequency in this system was low compared to what is used in industry[59], switching losses made for a large portion of the losses, as seen by the comparison of 62,5kHz and 31,25kHz switching. The reason why high frequencies are used is due to the fact that smaller inductors and capacitors are required, lowering equipment cost[60]. It should be noted that switching losses made for a large portion of the losses due to the lab scale circuit operating at relatively low voltages. Scaling the system up would naturally cause the switching losses to be a smaller percentage of the losses.

6.2 Conclusion

The use of second-life batteries as grid storage for peak shaving in commercial buildings is feasible and it is being explored, although it is far from commercial growth or maturity stages in the product life cycle.

The report explores the economic scenario for such a set-up serving a medium-sized supermarket in Denmark. Prices for batteries and electricity were accounted for, although the equipment setup could not be as closely estimated due to the hermetic nature of pricing information in highly-specialised B2B sellers. According to the estimates, the payback time could make the investment feasible under the best case scenario presented, if efficiencies are above 90%, which is achieved by many commercial solutions.

The equipment needed to make the second-life batteries take energy from the grid and supply it to the supermarket when required is known as BESS and can present multiple configurations. BESS are bidirectional, while the report focuses on the AC-DC conversion stage that provides a controllable DC output output to charge the batteries. An active single-phase rectifier in conjunction with a buck-boost DC-DC converter are simulated. The rectifier is of constant bus, therefore the controllable element is buck-boost. A mathematical model for it is derived and and a controller developed with mostly satisfactory results, although the inverted output of the buck-boost makes it an unlikely choice for an industrial application.

The DC-DC converter is also implemented in the laboratory with efficiency and control tests made. The control tests are, despite not meeting all specified goals, mostly satisfactory, whereas the efficiency obtained stretches the payback time obtained in the economic analysis beyond feasibility. A prototype with a closer-to-reality power demand could pro-

vide a higher output-power to switching-loss ratio, and the use of more complex converters that surpass the scope of this project, such as SEPIC, could be beneficial as well.

Bibliography

[1] Hauke Engel, Patrick Hertzke, and Guilia Siccardo. "Second-life EV batteries: The newest value pool in energy storage". In: (2019). URL: https://www.mckinsey.com/industries/automotive-and-assembly/our-insights/second-life-ev-batteries-the-newest-value-pool-in-energy-storage#/.

[2] Kadri Simson. *Commission Recommendation of 14 March 2023 on Energy Storage – Underpinning a decarbonised and secure EU energy system 2023/C 103/01*. 2023. URL: https://eur-lex.europa.eu/legal-content/EN/TXT/?uri=CELEX%3A32023H0320%2801%29&qid=1679302898964.

[3] Endesa.com. *Electric vehicle batteries that can light up a city*. 2020. URL: https://www.endesa.com/en/projects/all-projects/energy-transition/electric-vehicle-batteries-can-light-up-a-city.

[4] Asadullah Khalid, Alexander Stevenson, and Arif I. Sarwat. "Overview of Technical Specifications for Grid-Connected Microgrid Battery Energy Storage Systems". In: *IEEE Access* 9 (2021), pp. 163554–163593. DOI: 10.1109/ACCESS.2021.3132223.

[5] M.M. Samy et al. "Exploring energy storage methods for grid-connected clean power plants in case of repetitive outages". In: *Journal of Energy Storage* 54 (2022), p. 105307. ISSN: 2352-152X. DOI: https://doi.org/10.1016/j.est.2022.105307. URL: https://www.sciencedirect.com/science/article/pii/S2352152X22013056.

[6] Jian-Tang Liao et al. "BESS-Sizing Optimization for Solar PV System Integration in Distribution Grid". In: *IFAC-PapersOnLine* 51.28 (2018). 10th IFAC Symposium on Control of Power and Energy Systems CPES 2018, pp. 85–90. ISSN: 2405-8963. DOI: https://doi.org/10.1016/j.ifacol.2018.11.682. URL: https://www.sciencedirect.com/science/article/pii/S2405896318334013.

[7] Ujjwal Datta, Akhtar Kalam, and Juan Shi. "Smart control of BESS in PV integrated EV charging station for reducing transformer overloading and providing battery-to-grid service". In: *Journal of Energy Storage* 28 (2020), pp. 101–224. ISSN: 2352-152X. DOI: https://doi.org/10.1016/j.est.2020.101224. URL: https://www.sciencedirect.com/science/article/pii/S2352152X19310941.

[8] Fernando Núñez, David Canca, and Ángel Arcos-Vargas. "An assessment of European electricity arbitrage using storage systems". In: *Energy* 242 (2022), p. 122916. ISSN: 0360-5442. DOI: https://doi.org/10.1016/j.energy.2021.122916. URL: https://www.sciencedirect.com/science/article/pii/S0360544221031650.

[9] Andy Colthorpe. *Drive to rehabilitate New York City fossil fuel peaker plant sites with battery storage*. 2022. URL: https://www.energy-storage.news/drive-to-rehabilitate-new-york-city-fossil-fuel-peaker-plant-sites-with-battery-storage/.

[10] United Nations Department of Economic and Social Affairs. *Atmosphere*. URL: https://sdgs.un.org/topics/atmosphere (visited on 12/18/2023).

[11] Paul Denholm and Robert Margolis. *The Potential for Energy Storage to Provide Peaking Capacity in California under Increased Penetration of Solar Photovoltaics*. 2022. URL: https://www.energy-storage.news/drive-to-rehabilitate-new-york-city-fossil-fuel-peaker-plant-sites-with-battery-storage/.

[12] Hakan Polat et al. *A Review of DC Fast Chargers with BESS for Electric Vehicles: Topology, Battery, Reliability Oriented Control and Cooling Perspectives*. 2023. DOI: 10.3390/batteries9020121. URL: https://www.mdpi.com/2313-0105/9/2/121.

[13] Krunal Maniar. *Addressing high-voltage design challenges with reliable and affordable isolation technologies*. 2023. URL: https://www.ti.com/lit/wp/slyy204b/slyy204b.pdf?ts=1702854710280.

[14] Škoda. *Second-life battery hubs set to power up Škoda retailers*. 2021. URL: https://www.skoda.co.uk/news/details/second-life-battery-hubs-set-to-power-up-skoda-retailers.

[15] Aarian Marshall. *These Batteries Can't Power a Car—but They Can Light Up a City*. 2021. URL: https://www.wired.com/story/batteries-cant-power-car-light-city.

[16] California Energy Commission. *Reuse of Electric Vehicle Batteries for Solar Energy Storage*. Notice of Exemption. SCH Number 2020060627. 2020. URL: https://www.energy.ca.gov/programs-and-topics/documents/notice-exemption-2020060627.

[17] M Ridder. *Profit margin of Salling Group from 2012 to 2020*. 2021. URL: https://www.statista.com/statistics/778214/profit-margin-of-dansk-supermarked-group.

[18] Ben Hamilton. *Irma bites the dust in Coop reshuffle*. 2023. URL: https://cphpost.dk/2023-01-31/news/irma-bites-the-dust-in-coop-reshuffle.

[19] Reuters. *Norway's Reitan Retail buys 114 Danish stores from Germany's Aldi*. 2022. URL: https://www.reuters.com/markets/deals/norways-reitan-retail-buys-114-danish-stores-germanys-aldi-2022-12-09.

[20] dimsumdaily. *Denmark's supermarkets go dark in protest against sky-high energy costs*. 2022. URL: https://www.dimsumdaily.hk/denmarks-supermarkets-go-dark-in-protest-against-sky-high-energy-costs/.

[21] Danske Love. *Planloven. Lov om planlægning*. 2017. URL: https://danskelove.dk/planloven.

[22] John Field. "TM46 Energy benchmarks (2008)". In: *Chartered Institution of Building Services Engineers (CIBSE)* (2008).

[23] A. Foster, J. Evans, and G. Maidment. *Benchmarking of supermarket energy consumption.* 2018. DOI: 10.18462/IIR.ICCC.2018.0006. URL: http://iifiir.org/clientBookline/service/reference.asp?INSTANCE=EXPLOITATION&OUTPUT=PORTAL&DOCID=IFD_REFDOC_0023347&DOCBASE=IFD_REFDOC_EN&SETLANGUAGE=EN.

[24] Z. Mylona et al. "Comparative analysis on the energy use and environmental impact of different refrigeration systems for frozen food supermarket application". In: *Energy Procedia* (2017), pp. 121–130. URL: https://www.researchgate.net/publication/319947695_Comparative_analysis_on_the_energy_use_and_environmental_impact_of_different_refrigeration_systems_for_frozen_food_supermarket_application.

[25] S. M. van der Sluis. *Performance indicators for energy efficient supermarket buildings: Final report*. Tech. rep. HPTAN44-1. HPT Annex 44, 2017. URL: https://heatpumpingtechnologies.org/publications/performance-indicators-for-energy-efficient-supermarketbuildings-final-report/.

[26] SPAR International. *Average store size of SPAR International supermarkets worldwide in 2018, by country (in square meters)*. Retrieved October 03, 2023. Statista, 2020. URL: https://www.statista.com/statistics/728754/average-store-size-of-spar-international-supermarkets-worldwide-by-country/.

[27] Energinet Data Service. *Datahub Price List*. 2023. URL: https://www.energidataservice.dk/tso-electricity/DatahubPricelist.

[28] Skatteministeriet. *Elafgiftsloven*. 2023. URL: https://skm.dk/tal-og-metode/satser/satser-og-beloebsgraenser-i-lovgivningen/elafgiftsloven.

[29] Grand View Research Inc. *GVR Report cover Battery Market Size, Share Trends Analysis Report By Product (Lead Acid, Li-ion, Nickle Metal Hydride, Ni-Cd), By Application, By End-use, By Region, And Segment Forecasts, 2023 - 2030*. 2021. URL: https://www.grandviewresearch.com/industry-analysis/battery-market.

[30] Eurobat. *Avicenne study: "EU battery demand and supply (2019-2030) in a global context" shows that in the next decade lead and lithium batteries are critical to clean energy transition*. 2021. URL: https://www.eurobat.org/resource/avicenne-study-eu-battery-demand-and-supply-2019-2030-in-a-global-context-shows-that-%e2%80%8ein-the-next-decade-lead-and-lithium-batteries-are-critical-to-clean-energy-transition/.

[31] Yanyan Zhao et al. "A Review on Battery Market Trends, Second-Life Reuse, and Recycling". In: *Sustainable Chemistry* 2 (2021), pp. 167–205. URL: https://doi.org/10.3390/suschem2010011.

[32] Eurobat. *IEC Technical Committee 21 and its sub-committee 21A (IEC TC21/SC21A)*. 2023. URL: https://www.eurobat.org/what-we-do/topics-we-cover/standardisation/.

[33] European Commission. *COMMISSION STAFF WORKING DOCUMENT Accompanying the document REPORT FROM THE COMMISSION TO THE EUROPEAN PARLIAMENT AND THE COUNCIL Progress on competitiveness of clean energy technologies 6 7 - Batteries and Hydrogen Electrolyser*. 2021. URL: https://energy.ec.europa.eu/system/files/2021-10/swd2021_307_en_autre_document_travail_service_part4_v2.pdf.

[34] Mohammad Shahjalal et al. "A review on second-life of Li-ion batteries: prospects, challenges, and issues". In: *Energy* 241 (2021). URL: https://doi.org/10.3390/suschem2010011.

[35] J. Neubauer et al. "Identifying and Overcoming Critical Barriers to Widespread Second Use of PEV Batteries". In: *National Renewable Energy Laboratory* NREL/TP-5400-63332 (2015). URL: https://www.nrel.gov/docs/fy15osti/63332.pdf.

[36] Charlotte Argue. *What can 6,000 electric vehicles tell us about EV battery health?* 2019. URL: https://www.geotab.com/uk/blog/ev-battery-health/.

[37] Mike Dolzer. *Tesla Model 3 battery pack sized at 80.5 kWh according to EPA document*. 2017. URL: https://www.teslarati.com/tesla-model-3-battery-pack-size-epa/#:~:text=According%20to%20the%20EPA%20filing%2C%20the%20long%20range,Model%203%20uses%20an%2080.5%20kWh%20battery%20pack..

[38] Wall Street Journal. *Danish Krone, USDDKK (Tullett Prebon)*. 2023. URL: https://www.wsj.com/market-data/quotes/fx/USDDKK/historical-prices.

[39] Einar Berglund. *Grön Teknik 2023 - Vad händer med det gröna skatteavdraget?* 2023. URL: https://www.evify.se/artiklar/skatteavdrag-gron-teknik-2023/.

[40] TotalEnergies. *TEV is Banking on AutoGrid's Energy Flexibility Management Systems*. 2016. URL: https://totalenergies.com/news/tev-banking-autogrids-energy-flexibility-management-systems.

[41] Ahmad Alzahrani. "Experimental Investigation of Controlled and Uncontrolled Rectifiers for Low-Power Wind Turbines". In: *Applied Sciences* 13.7 (2023), pp. 4,6. ISSN: 2076-3417. DOI: 10.3390/app13074120. URL: https://www.mdpi.com/2076-3417/13/7/4120.

[42] Kummara Venkat Guru Raghavendra et al. *A Comprehensive Review of DC–DC Converter Topologies and Modulation Strategies with Recent Advances in Solar Photovoltaic Systems*. 2020. DOI: 10.3390/electronics9010031. URL: https://www.mdpi.com/2079-9292/9/1/31.

[43] Markus Zehendner and Matthias Ulmann. *Power Topologies Handbook*. Texas Instruments, 2023. URL: https://www.ti.com/seclit/ug/slyu036/slyu036.pdf.

[44] Dhrumil Daftary and Chirag H.Raval. "Controller Design for Buck–Boost Converter Using State-Space Analysis". In: *Renewable Energy and Climate Change* 161 (2019). DOI: 10.1007/978-981-32-9578-0_12. URL: https://link.springer.com/chapter/10.1007/978-981-32-9578-0_12.

[45] Taufiq Kurniawan Alif; Natajaya, Purnomo Aldyan; Priambodo Sidi; Wibisono, and Gunawan. "Real time monitoring state-of-charge battery using internal resistance measurements for remote applications". In: *Journal of Physics: Conference Series* 1528.1 (2020). ISSN: 1742-6588. DOI: 10.1088/1742-6596/1528/1/012034.

[46] Daniel W.Hart. *Power Electronics*. McGraw Hill, 2011. ISBN: 978-0-07-338067-4.

[47] Mamadou Diallo. *Bootstrap Circuitry Selection for Half-Bridge Configurations*. Application Note. Texas Instruments, 2023. URL: https://www.ti.com/lit/an/slua887a/slua887a.pdf?ts=1702166210460.

[48] ON Semiconductor. *FAN73711 High-Current, High-Side Gate Drive IC*. 2013.

[49] STMicroelectronics. *TL082, TL082A, TL082B General purpose JFET dual operation amplifiers*. 2016.

[50] Eric Guo Henry Xie. *How the Switching Frequency Affects the Performance of a Buck Converter*. 2019. URL: https://www.ti.com/lit/an/slvaed3/slvaed3.pdf.

[51] LLC Semiconductor Components Industries. *Application note: Design and Application Guide of Bootstrap Circuit for High-Voltage Gate-Drive IC*. 2021. URL: https://www.onsemi.com/pub/collateral/and9674-d.pdf.

[52] Fairchild Semiconductor. *FQP30N06L 60V LOGIC N-Channel MOSFET Datasheet*. 2013. URL: https://www.mouser.se/datasheet/2/308/1/FQP30N06L_D-2314160.pdf.

[53] Taiwan Semiconductor. *FR201 - FR207 2.0 AMPS. Fast Recovery Rectifiers*. URL: https://www.mouser.com/datasheet/2/395/FR201-231688.pdf.

[54] Mamadou Diallo. *Application Note: Bootstrap Circuitry Selection for Half-Bridge Configurations*. 2017. URL: https://www.ti.com/lit/an/slua887a/slua887a.pdf?ts=1702368293477.

[55] Mateo Begue. *Application Note: External Gate Resistor Design Guide for Gate Drivers*. 2020. URL: https://www.ti.com/lit/an/slla385a/slla385a.pdf?ts=1702409926445.

[56] Ali Shirsavar. *MOSFET Gate Drive Resistor Selection*. 2014. URL: https://www.youtube.com/watch?v=fsgKpAq2gd0&t=205s.

[57] David Forrest and Brett Beauregard. *Arduino-PID-Library - Version 1.2.3*. 2023. URL: https://github.com/drf5n/Arduino-PID-Library.

[58] electricity magnetism.org. *Buck-boost converter*. URL: https://www.electricity-magnetism.org/buck-boost-converter/#:~:text=High%20efficiency%3A%20By%20minimizing%20power%20losses%20during%20conversion%2C,converters%20can%20be%20designed%20with%20a%20minimal%20footprint. (visited on 12/15/2023).

[59] Eric Xie Henry Guo. *How the Switching Frequency Affects the Performance of Buck Converter*. 2019. URL: https://www.ti.com/lit/an/slvaed3/slvaed3.pdf?ts=1702735322039.

[60] Toke Meyer; Kamby Peter; Pedersen Jeppe Arnsdorf; Madsen Mickey Pierre;Kovacevic Milovan; Andersen Michael A. E Knott Arnold; Andersen. *Evolution of Very High Frequency Power Supplies*. 2013. URL: https://backend.orbit.dtu.dk/ws/portalfiles/portal/88233991/06680598.pdf.

Appendix A

Matlab Modelling Code

A.1 Matlab code for supermarket model

```
clc
clear all

s=tf('s')

%Output voltage
Vo = -350;

%Duty cycle setting
d = 0.5;
dd=1-d;

%Batteries internal resistance
R = 9.8;

%PWM pin arduino max speed
f = 62500;

%Inductance for BuckBoost Converter.
Lmin = (((dd)^2)*R)/(2*f);
L=1.25*Lmin


%Capacitance for BuckBoost Converter
```

```
25 ripplePercentage = 0.01;
26 Cmin=(d)/(ripplePercentage*R*f);
27 C=1.25*Cmin
28
29 %Boost direction of model
30 sys_continuous=(((Vo*dd*R)/(d))-(Vo*L*s)/dd)/((R*L*C*s^2)+(L*s)+((dd^2)*R))
31
32 %Analyzing the characteristics of the system
33 %pole(sys_continuous)
34 %zero(sys_continuous)
35 %step(sys_continuous)
36 %damp(sys_continuous)
37 %rlocus(sys_continuous)
38 %get(sys_continuous,'TimeUnit')
39 %step(feedback(sys_continuous, -0.00071));
40 BW = bandwidth(sys_continuous)/(2*pi)
41
42 %Controller and continuous system
43 Ki = -0.30907/s;
44 controlled_continuous_model = feedback(sys_continuous*(Ki), 1)
45 %step(controlled_continuous_model1);
46
47 %Setting Ts for discretization
48 nyquist_frequency = 2*BW;
49 realistic_sampling_frequency = 5*BW;
50 Ts = 1/realistic_sampling_frequency;
51
52 %Discretized model
53 controlled_discrete_model = c2d(controlled_continuous_model, Ts, 'ZOH')
54 %step(controlled_continuous_model,'-',controlled_discrete_model,'--');
55 %step(controlled_discrete_model)
```

A.2 Matlab code for prototype model

```
1 clc
2 clear all
3
4 s=tf('s')
5
```

```
%Duty cycle calculations
Vin = 10;
Vo_buck = -5;
Vo_boost = -15;
%Buck direction
d1 = -Vo_buck/(-Vo_buck + Vin);
dd1=1-d1
d2 = -Vo_boost/(-Vo_boost + Vin);
dd2=1-d2

%Batteries internal resistance
R = 1000;

%PWM pin arduino max speed
f = 62500;

%Inductance for BuckBoost Converter. We choose highest of both options
L1 = (((dd1)^2)*R)/(2*f);
L2 = (((dd2)^2)*R)/(2*f);
if L1 > L2
    Lmin = L1;
else
    Lmin = L2;
end
L=1*Lmin

%Capacitance for BuckBoost Converter
ripplePercentage = 0.01;
C1=(d1)/(ripplePercentage*R*f);
C2=(d2)/(ripplePercentage*R*f);
if C1 > C2
    Cmin = C1;
else
    Cmin = C2;
end
C=1*Cmin

%Boost direction of model. This was used to tune the controller.
sys_continuous_boost=(((Vo_boost*dd2*R)/(d2))-(Vo_boost*L*s)/dd2)/((R*L*C*s^2)+(L*s)+((dd2^2)*R))

%Contoller values for Arduino
%Ki=-11.55;
```

Appendix B

Arduino Prototype Code

```
#include <PID_v1_bc.h>

#define PIN_INPUT 0
#define PIN_OUTPUT 9

//duty cycle variable
int d;

//pwm variables
int pwm_value;
int pwm_to_pin;

//Variables to process ADC input to voltage value.
double ADC_measurement;
double actual_voltage;

//Op-Amp ratio, scaling and inverting the input to +5V max for the Arduino at a maximum output of -15V of the converter.
double Rf = 220.0;
double Rin = 670.0;
double Op_Amp_ratio = Rf/Rin;

//Voltage ADC ratio, stepsize for 10bit ADC up to 5V.
double VADC_ratio = 5.0/1024;

//Inverted voltage at output.
const double inv_V = -1.0;
```

```
27
28  //Define Variables for the PID
29  double Setpoint, Input, Output;
30
31  //Setting the limit of duty cycle for the controller. These were found experimentally based
    ↪  on what the circuit could handle.
32  //0.25 was where we reached the lower test bound of -5V. Above 0.65 the converter could not
    ↪  boost any more.
33  double d_min = 0.25;
34  double d_max = 0.65;
35
36  //Sample time of 1ms
37  int sample_time = 1;
38
39  //Measured correction factor of Voltage measurement compared to oscilloscope.
40  double correction_factor = 1.035;
41
42  //Specify the links and initial tuning parameters
43  double Kp=0, Ki=11.55, Kd=0;
44  PID myPID(&Input, &Output, &Setpoint, Kp, Ki, Kd, DIRECT);
45
46  void setup()
47  {
48    Serial.begin(9600);
49
50    //initialize the variables we're linked to
51    Input = analogRead(PIN_INPUT);
52    //Setpoint range is 5 to 13V.
53    Setpoint = 7;
54
55    // Configure Timer1 for Fast PWM mode(62.5kHz)
56    TCCR1A = (1 << COM1A1) | (1 << WGM11);
57    TCCR1B = (1 << WGM13) | (1 << WGM12) | (1<<CS10);
58    // Set the TOP value to 255 for 8-bit resolution
59    ICR1 = 255;
60
61    //Settings PID to autorun mode, setting duty cycle limit and setting sampling time.
62    myPID.SetMode(AUTOMATIC);
63    myPID.SetOutputLimits(d_min, d_max);
64    myPID.SetSampleTime(sample_time);
65  }
66
67  void loop()
68  {
```

```
69    pwm_to_pin = get_pwm_value();
70    analogWrite(PIN_OUTPUT, pwm_to_pin);
71  }
72
73  int get_pwm_value()
74  {
75    read_input();
76    myPID.Compute();
77    print_to_serial();
78    pwm_value = round(Output * 255);
79
80    return pwm_value;
81  }
82
83  void read_input()
84  {
85    ADC_measurement = analogRead(PIN_INPUT);
86    actual_voltage = ADC_measurement*VADC_ratio*inv_V*(1/Op_Amp_ratio)*correction_factor;
87    Input = -1*actual_voltage;
88  }
89
90  void print_to_serial()
91  {
92    Serial.print("Ref: ");
93    Serial.print(-1*Setpoint);
94    Serial.print("\tADC: ");
95    Serial.print(ADC_measurement);
96    Serial.print("\tV_out: ");
97    Serial.print(actual_voltage);
98    Serial.print("\tduty cycle: ");
99    Serial.print(Output);
100   Serial.print("\tPWM: ");
101   Serial.print(pwm_value);
102   Serial.println("");
103
104   //To check that controller has actually set the controller values
105   //Serial.print("\tKi: ");
106   //Serial.print(myPID.GetKi());
107 }
```